Tectonics

RESEARCH ARTICLE
10.1029/2022TC007692

Meso-Cenozoic Tectonic History of the Altai: New Insights From Apatite U-Pb and Fission Track Thermochronology for the Fuyun Area (Xinjiang, China)

Stijn Glorie[1], Angus L. Nixon[1], Gilby Jepson[1,2], Jack Gillespie[1,3], Cameron Warren[1], Fun Meeuws[1], Alexander Simpson[1], and Wenjiao Xiao[4,5]

[1]Department of Earth Sciences, University of Adelaide, Adelaide, SA, Australia, [2]Department of Geosciences, University of Arizona, Tucson, AZ, USA, [3]School of Earth and Planetary Sciences, The Institute for Geoscience Research (TIGeR), Curtin University, Perth, Australia, [4]State Key Laboratory of Lithospheric Evolution, Institute of Geology and Geophysics, Chinese Academy of Sciences, Beijing, China, [5]Xinjiang Research Centre for Mineral Resources, Xinjiang Institute of Ecology and Geography, Chinese Academy of Sciences, Urumqi, China

Abstract The Altai is an enigmatic, relatively young mountain belt with sharp relief (up to 4,500 m high) that developed thousands of kilometers away from the nearest current plate margins. The Fuyun area, at the interface between the southern margin of the Chinese Altai and the Junggar Basin, represents a key locality for understanding the Meso-Cenozoic deformation and exhumation history of the Altai. The complex structural architecture of the Fuyun area suggests that multiple deformation events affected the area, which ultimately led to the exhumation of the Altai. Furthermore, the area hosts orogenic-type mineralization, suggesting a history of fluid alteration. However, in contrast to the well-constrained Palaeozoic history, the timing of Meso-Cenozoic deformation, metasomatism and exhumation has not been comprehensively studied. This study presents new apatite U-Pb, trace element and fission track data for the Fuyun area and integrates these with previous studies for the Altai to shed more light on the Meso-Cenozoic tectonic history. The apatite U-Pb dates, associated with LREE-depleted trace element profiles, suggest that a phase of Middle–Late Jurassic (~170–160 Ma) metasomatism affected the Keketuohai area, which is potentially linked to the timing of rare-metal mineralization. The apatite fission track results and thermal history models reveal rapid early Late Cretaceous (~100–75 Ma) cooling linked to tectonic exhumation throughout the Chinese Altai, associated with distant plate-margin processes. In addition, samples taken in vicinity to the frontal thrusts of the Altai record evidence for Cenozoic partial resetting of the apatite fission track system.

Plain Language Summary The Altai Mountains are a high elevation, sharp relief mountain belt within central Asia. Despite their location thousands of kilometers from the present day plate margin, the Altai preserve young mountains induced by tectonic forces originating at the plate boundaries. Integrating new low-temperature data with existing studies reveals extensive uplift of the Altai during the Late Cretaceous, induced by the reactivation of major structures. A subsequent pulse of Cenozoic uplift further developed the topography observed today. In addition to mountain building, alteration of crystalline rocks associated with mineralization has also been observed. The chemical signatures within apatite grains suggests they grew from a fluid that altered the crystalline rocks, which may have links to nearby economic mineralization.

Key Points:

- The Fuyun area records Jurassic metasomatism in apatites corresponding to the timing of hydrothermal rare-metal mineralization
- Late Cretaceous rapid cooling is preserved throughout the Altai, coeval with km-scale deposition of coarse sediments in adjacent basins
- The Altai shows partial fission track resetting in the Cenozoic during India-Eurasia convergence, where exhumation has outpaced denudation

Supporting Information:

Supporting Information may be found in the online version of this article.

Correspondence to:

A. L. Nixon,
angus.nixon@adelaide.edu.au

Citation:

Glorie, S., Nixon, A. L., Jepson, G., Gillespie, J., Warren, C., Meeuws, F., et al. (2023). Meso-Cenozoic tectonic history of the Altai: New insights from apatite U-Pb and fission track thermochronology for the Fuyun area (Xinjiang, China). *Tectonics*, *42*, e2022TC007692. https://doi.org/10.1029/2022TC007692

Received 23 NOV 2022
Accepted 28 MAR 2023

Author Contributions:

Conceptualization: Stijn Glorie, Wenjiao Xiao
Formal analysis: Gilby Jepson, Jack Gillespie, Cameron Warren, Fun Meeuws, Alexander Simpson
Funding acquisition: Stijn Glorie, Wenjiao Xiao
Investigation: Stijn Glorie, Angus L. Nixon, Jack Gillespie, Cameron Warren, Fun Meeuws, Alexander Simpson
Resources: Wenjiao Xiao

1. Introduction and Regional Setting

The Altai is an intracontinental mountain range, which spans through eastern Kazakhstan, northwestern China, western Mongolia and southern Russia (Figure 1). Despite being located thousands of kilometers away from the nearest active continental convergence zone, the Altai intriguingly maintains high elevation, with peaks reaching up to 4,500 m. Located at the northwestern margin of the Central Asian Orogenic Belt (CAOB; Figure 1), the Altai are thought to represent the northern extremity of the deformation zone that was generated by the Cenozoic collision of India with Eurasia (e.g., De Grave et al., 2007; Molnar & Tapponnier, 1975), excluding only the Bikal Rift system and Sayan Mountains. Detailed structural, magmatic, geochronological, thermochronological and sedimentological studies, however, have revealed a polyphase deformation history spanning from the Palaeozoic to the latest Cenozoic (e.g., Briggs et al., 2007, 2009; Hendrix et al., 1992; Jolivet et al., 2007; Li, Yuan, et al., 2015; Yuan et al., 2006). Consequently, multiple tectonic episodes must be reconciled when considering the formation and preservation of such prominent intracontinental relief.

Visualization: Stijn Glorie, Angus L. Nixon, Gilby Jepson
Writing – original draft: Stijn Glorie, Angus L. Nixon, Gilby Jepson, Jack Gillespie
Writing – review & editing: Stijn Glorie, Angus L. Nixon, Gilby Jepson

Initiating in the late Palaeozoic, the Altai amalgamated from a series of accretions of island arcs, accretionary prisms, seamounts and microcontinents during the Cambrian–Carboniferous evolution of the Palaeo-Asian Ocean (Buslov et al., 2001, 2013; Glorie, De Grave, Buslov, Zhimulev, Izmer, et al., 2011; Windley et al., 2007), which culminated with the final closure of the Ob-Zaisan Oceanic realm in the late Carboniferous (Li et al., 2017). The closure of the Ob-Zaisan Ocean and the subsequent collision of the Altai with the Junggar terrane formed the Irtysh Shear Zone and induced extensive crustal thickening, magmatism, metamorphism, and transpressional strike-slip reactivation throughout both the Altai and the Tian Shan up to the Permian–Triassic (Briggs et al., 2007; Buslov et al., 2004; Glorie, De Grave, Delvaux, et al., 2012; Li, Sun, et al., 2015; Li, Yuan, et al., 2015; Li et al., 2017; Liu et al., 2012; Tong et al., 2014).

In contrast to the Palaeozoic tectonic history, the Mesozoic–Cenozoic intracontinental reactivation history of the Altai remains poorly understood. The low-temperature exhumation of the Altai has typically been attributed to far-field effects of strain propagation from the Mesozoic Eurasian plate margins, related to events of the Mongol-Okhotsk Orogeny (e.g., De Grave et al., 2009; van der Beek et al., 1996), or the collision and onset of subduction of the Kohistan-Ladakh Arc terranes at the Tethys margin (e.g., Hendrix et al., 1992; Yuan et al., 2006), and progressive, ongoing collision between India and Eurasia (e.g., A. Li et al., 2022; C. Li et al., 2022; Yuan et al., 2006). Additionally, enigmatic Triassic–Jurassic anorogenic intraplate magmatism is widespread within the Altai, with a variety of tectonic settings suggested for their origin; from an extensional setting to a far-field effect of the Siberian plume (Liu & Han, 2019; Wang et al., 2014). Furthermore, Au-Cu-Pb-Zn-rare metals mineralization within the Chinese Altai has been linked to widespread Mesozoic fluid alteration. However, age constraints on such fluids in the Altai are limited to mined deposits and often debated (Liu et al., 2014; Xue et al., 2016; Zheng et al., 2017; Zhou et al., 2015), yet are crucial for more robust understanding of the evolution and mineralization of the region.

This study presents a combination of zircon LA–ICP–MS (ZUPb) and apatite U-Pb (AUPb) geochronology, apatite fission track (AFT) thermochronology and apatite trace element geochemistry from the Fuyun area of the Chinese Altai (Figure 2) to illuminate the regional Meso–Cenozoic intracontinental evolution. The Fuyun area provides an optimal study region due to the occurrence of Mesozoic magmatic rocks and orogenic Cu-Au-rare metals mineralization (Liu et al., 2014; Liu & Han, 2019; Xue et al., 2016; Zhou et al., 2015), and the presence of a network of faults (Figure 2) that are thought to have been reactivated during the Cenozoic (Cunningham et al., 2003). The AUPb geochronology and trace element geochemistry are used to explore the post-magmatic history of the study area (e.g., metasomatism in relation to mineralization), using ZUPb ages as a reference for primary magmatism. Additionally, the new AFT data set is integrated with published AFT, U-Th-Sm/He and Ar-Ar data (Figures 1 and 2) to provide a review of the Mesozoic exhumation and deformation history of the Altai, and to evaluate if the Altai record thermochronological evidence for Cenozoic deformation.

2. Geological Setting

The Altai Mountains formed through a prolonged Palaeozoic accretion along the southern margin of the Siberian Craton (Windley et al., 2007). The southern Siberian Craton comprised of a passive continental margin, on to which terrigenous clastic sedimentary rocks were deposited (Chang et al., 1995; Windley et al., 2002). During the early Palaeozoic, the passive continental margin transitioned into an active margin in response to the north-dipping subduction of the Ob-Zaisan Ocean (Chen & Jahn, 2002; Windley et al., 2002), which led to associated early to mid-Palaeozoic arc-magmatism and subduction complex accretion (e.g., Li et al., 2017; Xiao et al., 2009). This culminated with the closure of the Ob-Zaisan Ocean, which accreted the Junggar intra-oceanic arc system to the Altai in the late Carboniferous (e.g., Li et al., 2017; Xiao et al., 2009).

The Carboniferous suture between the Altai and the Junggar corresponds to the Irtysh Shear Zone (e.g., Briggs et al., 2007; Laurent-Charvet et al., 2002; Xiao et al., 2015). From the late Carboniferous to the Permian, the Irtysh Shear Zone hosted three episodes of deformation, responsible for mylonitisation, orogen parallel extension, and transpression (Briggs et al., 2007, 2009; Hu et al., 2020; Li, Sun, et al., 2015; Li et al., 2017; Zhang et al., 2012). Permian deformation along the Irtysh Shear Zone caused considerable shortening and crustal thickening, as evidenced by elevated La/Yb ratios in syn-tectonic granitoids (e.g., Tong et al., 2014). Despite prolonged Mesozoic–Cenozoic tectonic activity, upper-crustal exhumation in response to Permian shortening along the Irtysh Shear Zone is still preserved in the west Junggar mountains (Gillespie et al., 2020). Numerous granitic intrusions in the Fuyun area, here defined as the intersection

10.1029/2022TC007692

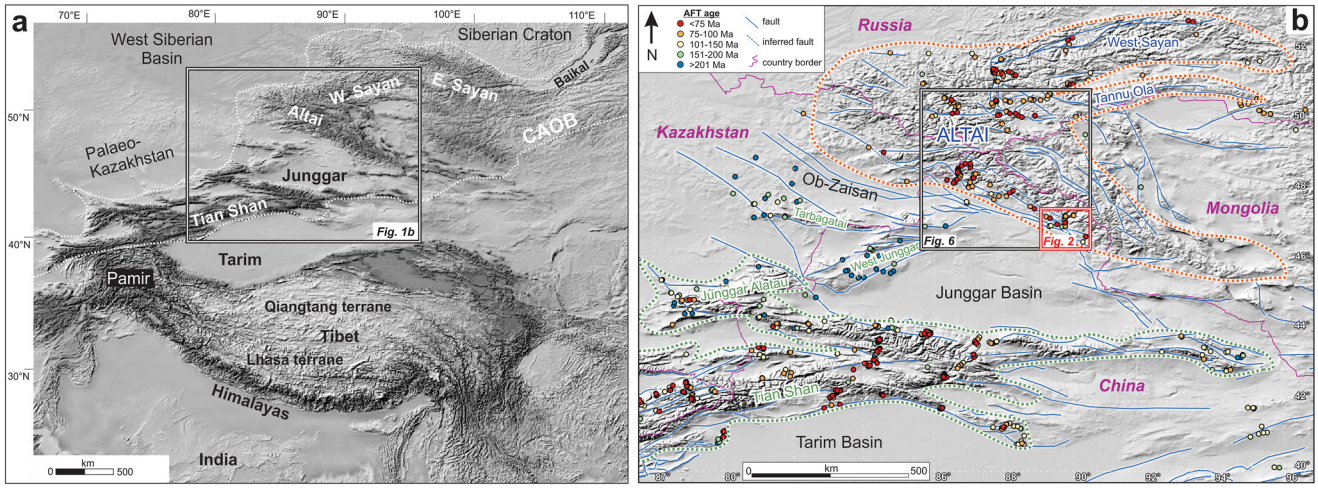

Figure 1. (a) Overview topographic map for Central Asia with indication of the main basins and mountain ranges within the Central Asian Orogenic Belt (CAOB—white dotted outline). (b) Digital elevation model for the central part of the CAOB, focused on the Altai-Sayan (outlined blue dotted outline), with indication of published apatite fission track (AFT) sample locations, color-coded to AFT ages (data from De Grave & Van den haute, 2002; De Grave et al., 2008, 2009, 2013, 2014; De Pelsmaeker et al., 2015; Dumitru et al., 2001; Gillespie, Glorie, Jepson, et al., 2017; Gillespie, Glorie, Xiao, et al., 2017; Gillespie et al., 2020, 2021; Glorie et al., 2010; Glorie, De Grave, Buslov, Zhimulev, Stockli, et al., 2011; Glorie, De Grave, Buslov, et al., 2012; Glorie, De Grave, Delvaux, et al., 2012; Glorie, Otasevic, et al., 2019; Jolivet et al., 2007, 2010, 2013; Macaulay et al., 2014; Nachtergaele et al., 2018; Pullen et al., 2020; Vassallo et al., 2007; Wang et al., 2009, 2018; Yuan et al., 2006; Zhang et al., 2009, 2016). Major faults are shown, based on structural maps from Cunningham (2007), Mohadjer et al. (2015, 2016).

zone between the ~E-W striking Irtysh Shear Zone and the roughly N-S striking Fuyun strike-slip fault (Figure 2), preserve varied deformational histories. Devonian granitoids preserve deformation fabrics and are often associated with the greenschist to amphibolite facies Irtysh Complex in the Fuyun area (Li et al., 2017; A. Li et al., 2022; C. Li et al., 2022). Permian aged granites are commonly undeformed (Li, Sun, et al., 2015; Sun et al., 2008; Tong et al., 2014), as are several Mesozoic granitoids documented throughout the Altai (Li et al., 2013; Liu et al., 2014).

Late Permian–Jurassic monazite U-Pb ages and biotite Ar-Ar cooling ages recorded in the Altai suggest exhumation of up to 20 km in relation to thrust faulting in the early to mid-Mesozoic (Briggs et al., 2009; Li, Yuan, et al., 2015). Mesozoic exhumation is contemporaneous with the emplacement of mixed continental and juvenile Late Triassic–Jurassic plutonism in the Altai (Wang et al., 2014). In the mid to Late Cretaceous, the southern Altai cooled to upper-crustal temperatures (~120–40°C), corresponding to depths of ~2–6 km (Pullen et al., 2020; Yuan et al., 2006). This Late Cretaceous period of upper-crustal cooling is associated with the development of an unconformity in the northern Junggar Basin and the subsequent deposition of conglomerate layers within the Donggou Formation (Hendrix et al., 1992; Vincent & Allen, 2001). Within the Altai, the Late Cretaceous unconformity and upper-crustal exhumation have been attributed to collision-accretion processes on the southern Eurasian margin, causing contraction and deformation in the Eurasian hinterland (Hendrix et al., 1992; Yuan et al., 2006). However, Late Cretaceous exhumation is not just restricted to the southern Altai. Numerous researchers have documented consistent, Late Cretaceous low-temperature cooling ages from eastern Kazakhstan to Lake Baikal in south-eastern Siberia (Figure 1) (De Grave et al., 2007, 2009, 2014; Glorie, De Grave, Buslov, et al., 2012, Glorie, De Grave, Delvaux, et al., 2012; Jolivet et al., 2007, 2013; van der Beek et al., 1996; Vassallo et al., 2007). Several authors have considered a long-wavelength, regional tectonic process such as orogenic collapse (e.g., De Grave et al., 2014) or modification to the continental hydroclimate (e.g., McDannell et al., 2018; Pullen et al., 2020) as responsible for this regional Late Cretaceous cooling signal.

Despite the regional preservation of Late Cretaceous exhumation throughout the Altai, it is generally considered that much of the modern topography formed in response to deformation caused by the India-Asia collision (e.g., Molnar & Tapponnier, 1975; Sobel et al., 2006). In the Altai Mountains, increased strain due to the ongoing India-Asia collision reactivated pre-existing basement structures and generated widespread uplift (Jolivet et al., 2007; Vassallo et al., 2007; Yuan et al., 2006). The development of elevated topographic relief is assessed to have onset in the early Miocene in both the eastern Tian Shan (e.g., Hendrix et al., 1994; Lü et al., 2013) and the southern Altai (e.g., Hendrix et al., 1992).

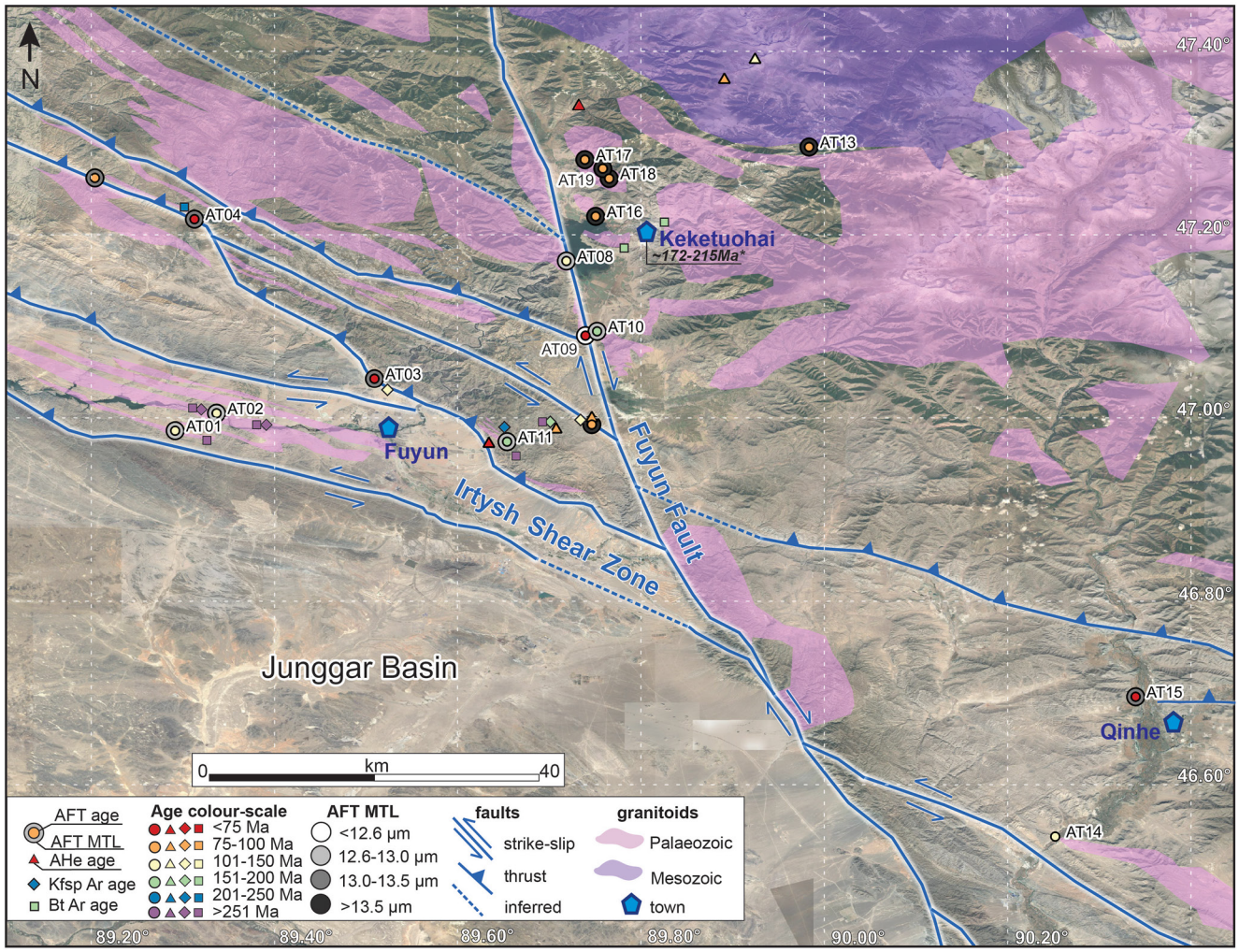

Figure 2. Google Earth map of the study area, with indication of granitoid outcrops and major structures and their kinematics (after Briggs et al., 2007; Li, Sun, et al., 2015; Li, Yuan, et al., 2015). New sample locations from this study are named and both new and previously published sample symbols are color-coded following their apatite fission track (AFT) central ages (circle symbols) or mean apatite U-Th-Sm/He (AHe) ages (triangle symbols), K-feldspar ^{40}Ar-^{39}Ar ages (diamond symbols) and biotite ^{40}Ar-^{39}Ar ages (square symbols) (data from Briggs et al., 2007, 2009; Li, Yuan, et al., 2015; Pullen et al., 2020; Yuan et al., 2006). The range of zircon U-Pb and molybdenite Re-Os ages for the Keketuohai pegamatitic rare earth elements deposit are also indicated (Liu & Han, 2019; Liu et al., 2014; Zhou et al., 2015). Mean confined fission track length (MTL) data are displayed as a gray-scale outline around the circle symbols (with darker outlines representing higher MTL values, reflecting fast cooling and absence of secondary thermal events).

3. Sample Descriptions

Samples AT-01 and AT-02 were collected from the migmatitic Irtysh Complex along the Irtysh Shear Zone (Figure 2; Li et al., 2017). Sample AT-01 is a coarse-grained gneiss, containing abundant 3–4 mm plagioclase and quartz. The foliated fabric is defined by biotite and minor garnet. Sample AT-02 is a strongly foliated orthogneiss with abundant biotite, plagioclase and quartz, commonly intruded by coarse dikes. The sample location for AT-01 yielded a published SHRIMP ZUPb date of 281 ± 5 Ma (Tong et al., 2014). For AT-02, there is no published crystallisation age available in the literature beyond that the Irtysh Complex is Devonian–early Carboniferous in age, and was cross-cut by Permian dikes (Li, Sun, et al., 2015; Li et al., 2017).

Samples AT-03 and AT-04 were collected from a strongly foliated orthogneiss in the metamorphosed volcanic and sedimentary sequence of the Altai Formation (Li, Sun, et al., 2015) along an unnamed thrust fault, north of the Irtysh Fault (Figure 2). Both rocks contain abundant biotite, which defines the foliation, as well as quartz and plagioclase. The orthogneiss yields an Early Triassic biotite ^{40}Ar-^{39}Ar age (~245 Ma), near the sample locality for AT-04 (Li, Sun, et al., 2015 and references therein). Sample AT-11 was collected from the same thrust as samples AT-03 and AT-04 (near Fuyun town), but more distal to the fault (Figure 2). Sample AT-11 was collected

from a porphyritic granitoid with large K-felspar phenocrysts in a matrix of plagioclase, quartz and biotite, which intrudes amphibolites. Published literature on the porphyritic granitoid reports a metamorphic zircon U-Pb age of ~277 Ma and a biotite ^{40}Ar-^{39}Ar age of ~265 Ma (Li, Sun, et al., 2015 and references therein).

Samples AT-08, AT-09, and AT-10 were taken from middle Palaeozoic granodiorites along the Fuyun Fault, north of Fuyun town (Figure 2). Sample AT-08 was sourced from a large granodiorite outcrop to the west in close proximity of the Fuyun Fault, and lacks a foliation fabric. Sample AT-09 was sampled at the intersection between the Fuyun Fault and an unnamed thrust fault and is an orthogneiss defined by a biotite fabric. Sample AT-10, sampled on the eastern side of the Fuyun Fault, is an unfoliated granodiorite containing large plagioclase and quartz phenocrysts with minor biotite.

Samples AT-16, AT-17, AT-18, and AT-19 were collected from a granitoid with large plagioclase phenocrysts to the east of the Fuyun Fault, near Keketuohai town (Figure 2). Sample AT-16 has abundant biotite, while the micas in samples AT-18 and AT-19 are predominantly muscovite. Sample AT-17 has a dioritic composition with plagioclase phenocrysts in a dark aphanitic groundmass. The granodiorite outcrops are mapped as Devonian in age and are intruded by abundant Late Triassic (~212–209 Ma) granitic pegmatites that were mined for rare earth elements (REE) (Liu & Han, 2019; Liu et al., 2014). Absolute age constraints are not available in published literature for these sample locations. Sample AT-13 was taken farther east, from a foliated orthogneiss at the boundary of the Triassic (~212–210 Ma) Alaer (also named Aral) intrusion (Liu & Han, 2019; Liu et al., 2014).

Samples AT-14 and AT-15 were taken in the southeast of the study area (Figure 2). Sample AT-14 is a biotite orthogneiss with a published ZUPb date of 283 ± 4 Ma (Tong et al., 2014). Sample AT-15 was sourced from a Permian felsic dike near the Qinghe town (Figure 2). Due to logistical issues, hand-samples of lithologies analyzed in this study were unavailable for detailed thin-section petrographic analysis.

4. Methods

4.1. Mineral Separation and Zircon U-Pb Analysis

Zircon and apatite separates were obtained from the samples by crushing, sieving and heavy liquid separation at the Institute of Geology and Geophysics, Chinese Academy of Sciences (IGGCAS). At The University of Adelaide, the zircon and apatite grains were mounted in EpoxyCure resin onto thin section slides and then ground and polished to expose internal sections of the grains. ZUPb ages were calculated to provide accurate constraints on the timing of crystallisation for each sampled intrusion that had no published ZUPb dates available. Zircon target sites for U-Pb isotopic analyses were chosen from cathodoluminescence (CL) images, carried out using an FEI Quanta 600 Scanning Electron Microscope equipped with a tungsten filament electron source and a Gatan CL detector at Adelaide Microscopy.

ZUPb analyses were performed by laser ablation inductively coupled mass spectroscopy (LA-ICP-MS) at Adelaide Microscopy using a New Wave UP-213 laser ablation system coupled to an Agilent 7900 ICPMS system. Instrument and mass calibration were performed prior to all analytical sessions using the NIST 612 reference glass by maximizing the ^{238}U signal and by minimizing oxide formation using the ThO+/Th + ratio (<1%). U-Pb-Th isotope fractionation was corrected using the GEMOC GJ-1 standard (^{206}Pb/^{238}U age of 600.7 ± 1.1 Ma; 2σ) (Jackson et al., 2004) and internal accuracy was monitored using the Plešovice zircon standard (^{206}Pb/^{238}U age of 337.1 ± 0.37 Ma; 2σ) (Sláma et al., 2008). The zircon data were processed in Iolite (Paton et al., 2011) and plotted in IsoplotR (Vermeesch, 2018). Plešovice analyses yield a weighted average ^{206}Pb/^{238}U age of 337.7 ± 1.1 Ma (2σ; MSWD = 1.0; n = 29, Supporting Information S1).

4.2. Apatite U-Pb and Trace Element Analysis

Trace element concentrations and U–Pb isotopes from grain mounted apatites were measured on a RESOlution-LR 193 nm excimer laser coupled to an Agilent 7900 ICPMS system, following the analytical procedures and identical instrumental settings as outlined in Gillespie et al. (2018) and Glorie et al. (2020). Data reduction was carried out using the "VisualAge_UcomPbine" and "X_Trace_Elements_IS" data reduction software packages for Iolite (Paton et al., 2011) and IsoplotR was used for U-Pb age calculations (Vermeesch, 2018). Regression lines in Tera-Wasserburg plots were all unanchored to allow age calculations without assumptions about the initial (common) Pb isotopic composition (cf. Glorie, Jepson, et al., 2019; Kirkland et al., 2018). Madagascar apatite (MAD; ID-TIMS age of 473.5 ± 0.7 Ma; Chew et al., 2014; Thomson et al., 2012) was used as the primary

reference material for AUPb age calculations and NIST610 glass was used as the primary standard for trace element concentration determinations. McClure and Durango apatites were used as secondary reference material, yielding ^{207}Pb-corrected weighted average ages of 528 ± 6 Ma (2σ; MSWD = 1.3; n = 18, Supporting Information S1) and 30.9 ± 1.3 Ma (2σ; MSWD = 1.0; n = 17, Supporting Information S1), respectively. These value are in good agreement with the published ID-TIMS ^{207}Pb/^{235}U age for McClure apatite of 523.51 ± 1.47 Ma (Schoene & Bowring, 2006) and the published ^{40}Ar/^{39}Ar age of 31.44 ± 0.18 Ma (McDowell et al., 2005). REE concentrations in apatite were normalized against primitive mantle values (McDonough & Sun, 1995) and displayed on spider plots (using GCDkit, Janousek et al., 2006). Multi-element discrimination principal component analysis (PCA) and multiclass support vector machine classification were used to categorize the samples based on apatite trace-element geochemistry by comparing the apatite trace element data with an extensive published apatite geochemistry database (O'Sullivan et al., 2020; O'Sullivan et al., 2018).

4.3. Apatite Fission Track Analysis

AFT data record the thermal history of the samples through the apatite partial annealing zone (APAZ) (~60–120°C) (Wagner et al., 1989). Etching of the samples was completed in a solution of 5.5 M HNO_3 for 20 ± 0.5 s at 20 ± 0.5°C to reveal the spontaneous fission tracks, following Glorie et al. (2017). Imaging of individual grains from each sample was conducted on a Zeiss AXIO Imager M2m Autoscan System with a magnification of x1000. Following imaging, fission track densities and confined track lengths in the individual grains were measured using the FastTracks software. ^{238}U concentration measurements were obtained simultaneously with U-Pb isotope analysis (outlined above) and fission track ages were calculated in IsoplotR (Vermeesch, 2018) using a zeta-calibration based on Durango apatite (Hasebe et al., 2013; McDowell et al., 2005; Vermeesch, 2017). The weighted average AFT age for Durango apatite in this study was calculated as 31.1 ± 4.0 Ma (2σ; MSWD = 0.3; n = 17, Supporting Information S1), which is within uncertainty of the published ^{40}Ar/^{39}Ar age of 31.44 ± 0.18 Ma (McDowell et al., 2005), suggesting reliable fission track results. Where feasible, a ^{252}Cf irradiation was conducted at The University of Adelaide to increase the number of measurable confined fission tracks (e.g., Donelick & Miller, 1991; Gillespie et al., 2020).

4.4. Thermal History Modeling

Thermal history models were constructed using QTQt software version 5.6.0 (Gallagher, 2012). AUPb ages were introduced into the modeling, reflecting temperatures of 400 ± 50°C (e.g., Cherniak, 2010). The modeling procedure involved running 10,000 possible models as a test run to gauge the plausibility of thermal history models. Models deemed as geologically representative and statistically acceptable, as evaluated by agreement between observed and predicted residuals, were further refined by running an extra 50,000 possible models. Detailed modeling parameters and residuals for each sample are tabulated in Supporting Information S1, following the reporting protocol from Flowers et al. (2015).

5. Results

5.1. Zircon and Apatite U-Pb Dates and Apatite Trace-Element Geochemistry

Zircon and apatite U-Pb results are summarized in Table 1. The U-Pb isotope ratios used to derive the zircon ages are listed in Supporting Information S2 (https://doi.org/10.25909/21590265), and U-Pb isotope ratios for apatite are provided in Supporting Information S3 (https://doi.org/10.25909/21590286). The trace element geochemistry for each single-grain apatite and zircon analysis can be found in Supporting Information S4 (https://doi.org/10.25909/21590292). ZUPb concordia plots and weighted mean plots that were used for the age calculations, as well as AUPb Tera-Wasserburg concordia plots and apatite normalized REE trace-element plots are presented in Supporting Information S1.

Samples AT-01, AT-02, AT-03, AT-04, AT-14, and AT-15 from the migmatitic Irtysh Complex and Altai Formation record Permian (~287–272 Ma) ZUPb crystallisation ages. These are consistent with published zircon ages for the respective units (281 ± 5 and 283 ± 4 Ma) (Tong et al., 2014). The obtained AUPb ages are all younger than corresponding ZUPb ages and range between ~268 and 260 Ma for samples AT-01, 02, 03, 14, 15, while AT-04 records a slightly younger age of ~238 Ma. Apatite REE spiderplots record flat or negatively sloping LREE patterns that are particularly strongly pronounced for samples AT-03 and AT-14 (Supporting Information S1). Samples AT-02, AT-04, and AT-15 show low total REE concentrations. AT-11 yields an AUPb age

Table 1
Sample Details (Long. = Longitude, Lat. = Latitude) and Zircon/Apatite Geochronology

Sample	Long.	Lat.	Altitude (m)	Published age [Ma]	Zr U-Pb age [Ma]	N	MSWD	Ap U-Pb age [Ma]	n	MSWD
AT-01	89.2915	46.9859	844	281 ± 5	–	–	–	262 ± 19	4	3.3
AT-02	89.3367	47.005	752	Permian	*430 ± 2*	*15*	*2.9*	268 ± 7	19	0.8
					287 ± 4	4	3.9			
AT-03	89.5093	47.043	1,107	Permian	278 ± 1	30	4.4	260 ± 13	15	0.7
AT-04	89.3126	47.217	1,029	Permian	280 ± 2	21	1.1	238 ± 8	20	3.6
					262 ± 3	*5*	*2.4*			
AT-08	89.7187	47.1714	1,286	mid-Pz.	383 ± 3	18	4.4	334 ± 31	15	1.4
AT-09	89.7395	47.09	1,332	mid-Pz.	–	–	–	–	–	–
AT-10	89.7522	47.0947	1,257	mid-Pz.	–	–	–	412 ± 55	6	0.6
AT-11	89.654	46.974	1,020	257 ± 5	–	–	–	252 ± 16	14	1.3
AT-13	89.9834	47.2957	1,565	mid-Pz.	388 ± 2	24	3.2	159 ± 3	16	2.7
AT-14	90.2519	46.5434	1,173	283 ± 4	–	–	–	263 ± 34	9	1.5
AT-15	90.3396	46.6958	1,298	Permian	272 ± 5	5	1.5	267 ± 7	16	3.0
AT-16	89.7507	47.2201	1,167	mid-Pz.	395 ± 3	19	2.4	169 ± 22	8	2.1
AT-17	89.7389	47.2819	1,457	mid-Pz.	210 ± 2	10	2.4	165 ± 51	16	1.3
					193 ± 5	*4*	*1.1*			
AT-18	89.7654	47.2613	1,996	mid-Pz.	212 ± 1	20	1.8	198 ± 20	9	2.9
AT-19	89.7584	47.2722	1,740	mid-Pz.	–	–	–	175 ± 17	10	1.6

Note. Published ages are derived from Tong et al. (2014) and references therein. Where no zircon dates were available, time periods were inferred from geological maps. Zircon (Zr) and apatite (Ap) U-Pb dates are reported with their 95% confidence uncertainties. The reported zircon U-Pb dates are weighted mean $^{206}Pb/^{238}U$ ages, the apatite U-Pb dates are lower intercept ages from Stacey and Kramers concordia plots (both calculated in IsoplotR (Vermeesch, 2018)). Where multiple zircon populations could be calculated, the interpreted crystallization ages are given in standard font and interpreted ages for inherited or altered populations are given in italic font. *N* = number of analyzed zircons, *n* = number of analyzed apatites. MSWD = mean square weighted deviation (which is a measure of goodness of fit).

of 252 ± 16 Ma, which corresponds well to a published ZUPb date for the same intrusive (257 ± 5 Ma; Tong et al., 2014). Samples AT-08, AT-09, and AT-10 were sampled from granitoids along the Fuyun Fault (Figure 2) that are mapped to be Devonian in age. They show similar flat apatite REE profiles with strong Eu anomalies. For sample AT-08, a ZUPb age of 383 ± 3 Ma was obtained, while for other samples no zircons could be retrieved. The AUPb age for AT-08 is slightly younger (334 ± 31 Ma) than its zircon age and sample AT-10 records an imprecise older AUPb age (412 ± 55 Ma). Samples AT-13, AT-16, AT-17, AT-18, and AT-19 were taken from a combination of granitoids that are mapped to be Devonian in age and cross-cutting pegmatitic outcrops near the Keketuohai mines. Samples AT-13 and AT-16 record zircon U-Pb ages of 388 ± 2 Ma and 395 ± 3 Ma, respectively. Samples AT-17 and AT-18 record ~212–210 Ma zircon crystallisation ages, and for AT-19 no crystallisation age could be obtained due to the lack of zircons. The AUPb dates for these samples are the youngest in the study area and range between ~198 Ma and ~159 Ma. Sample AT-18 produced the oldest AUPb age for this group of samples, which overlaps within uncertainty with its ZUPb age, and is characterized by a flat apatite REE trend. All other samples in this group record negatively sloping LREE profiles.

The age and trace element geochemistry datasets are summarized in Figure 3. The zircon versus apatite U-Pb age plot reveals significant offsets between the two chronometers that are correlated with relatively low normalized La/Sm ratios (a measure for negatively sloping LREE profiles). In more detail, samples AT-03 and AT-14 record AUPb ages of ~260 Ma associated with very low (~0.2–0.05) normalized La/Sm ratios. Similarly, the youngest AUPb dates for the study area (~175–159 Ma) are significantly younger than their corresponding zircon ages, and are associated with low normalized La/Sm ratios of ~0.5–0.2. This suggests that the apatites (re)crystallized with a competing mineral for LREEs. On a LREE (La + Ce + Sm + Nd) versus Sr/Y geochemical biplot (Mao et al., 2016; O'Sullivan et al., 2020), the individual analyses for the samples from this study define a series of

10.1029/2022TC007692

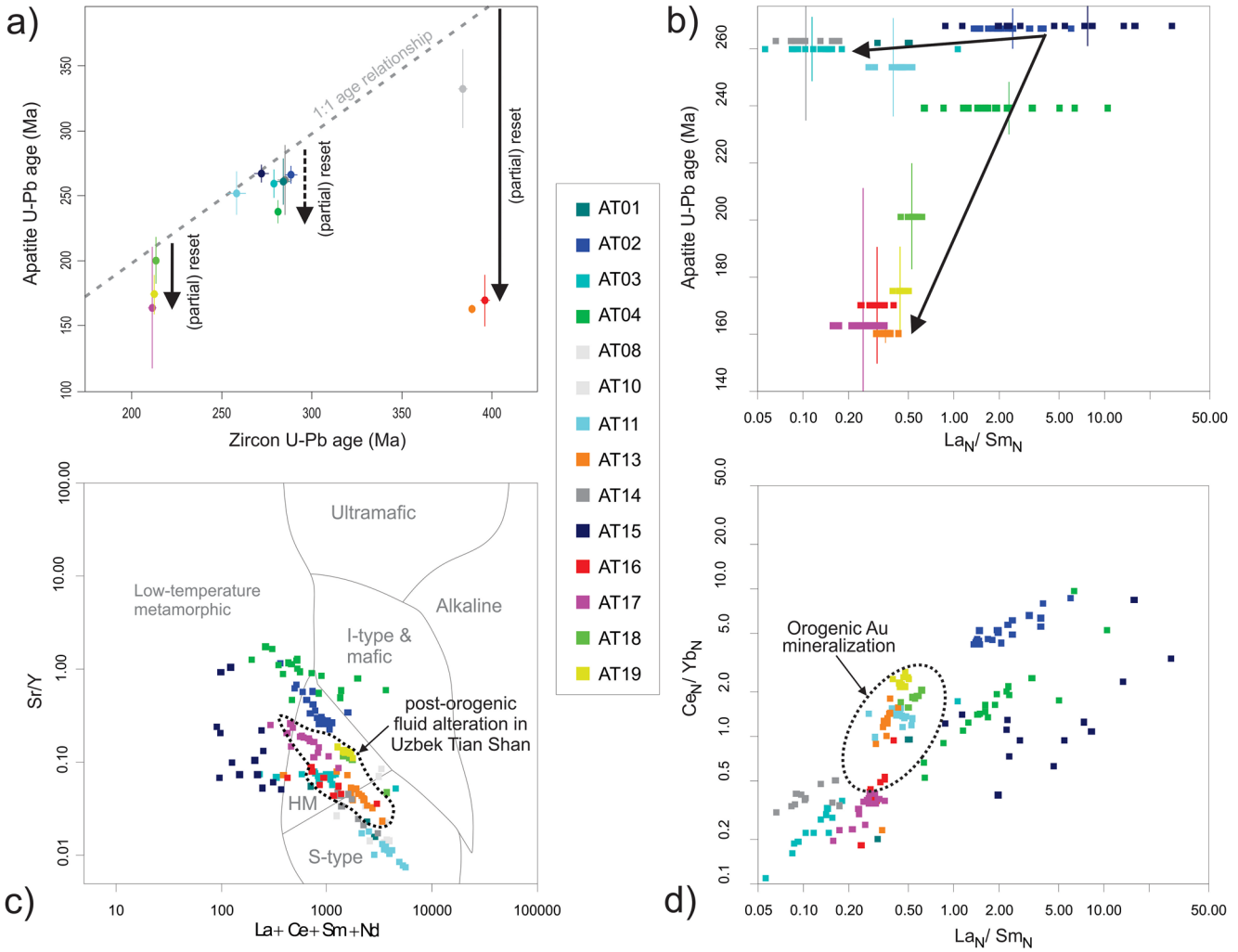

Figure 3. (a) Comparison plot of zircon and apatite U-Pb dates for the samples in this study. Several samples deviate from the 1:1 age relationship, suggesting that the apatite U-Pb dates record partial resetting in relation to a thermal process (metamorphism) or fluid alteration. Samples that record most significant resetting consistently record apatite U-Pb ages of ~180–160 Ma, regardless of the age of the sampled grantioids. (b) Primitive mantle normalized La/Sm versus apatite U–Pb age plot (cfr. Glorie, Jepson, et al., 2019) reveals a trend to low La/Sm ratios at ~265–250 Ma and at ~180–160 Ma, suggesting that, at these times, apatites grew or recrystallized together with a competing mineral for LREEs. (c) LREE (La + Ce + Sm + Nd) versus Sr/Y geochemical biplot for apatite with indication of petrogenetic fields (Mao et al., 2016; O'Sullivan et al., 2020). The individual analyses for the samples from this study define a series of linear trends that span across the S-type granite, high-temperature metamorphic (HM) and low-temperature metamorphic fields, suggesting they record a signature of metamorphic and/or fluid-related alteration. The trace element geochemistry for the samples with the youngest (<200 Ma) apatite U-Pb ages (light green, yellow, red, purple, orange symbols) correspond closely to those recording post-orogenic fluid alteration in the Uzbek Tian Shan (dotted outlined field, based on data from Glorie, Jepson, et al. (2019), displayed in Supporting Information S1). (d) Normalized La/Sm versus Ce/Yb plot showing that the trace-element geochemical signatures for the young apatite samples from this study (apatite U-Pb dates <200 Ma) can be correlated with those for apatite samples from orogenic Au deposits in British Columbia and the Uzbek Tian Shan (dotted outlined field, based on data from Mao et al. (2016) and Glorie, Jepson, et al. (2019), displayed in Supporting Information S1).

linear trends that span across the S-type granite, high-temperature metamorphic and low-temperature metamorphic fields, suggesting that they record a signature of metamorphic and/or fluid-related alteration.

5.2. Apatite Fission Track Data and Modeling

The AFT results are presented in Table 2, on radial plots and confined fission track length histograms (Supporting Information S1). The AFT data for individual grains can be accessed via Supporting Information S5 (https://doi.org/10.25909/21590310).

The AFT central ages for this study range between ~157 Ma and ~60 Ma. While most samples pass the chi-squared test and can thus be treated as statistically single population samples, some show over-dispersion without clear correlation to variations in apatite Cl (Green et al., 1986) or U (Fernie et al., 2018) chemistry or D_{par} values

Table 2
Apatite Fission Track (AFT) Age and Length Details

Sample	ρ_s [×10^6] (1SE)	Ns	N	^{238}U [ppm] (1SE)	Central age [Ma] (1SE)	P(χ^2)	Disp. [%]	l_m [μm]	n	σ_c [μm]	Cl [wt%]
AT-01	7.57 (0.60)	322	3	99.0 (2.2)	146 ± 8	0.51	0.0	12.63	45*	1.17	0.06 (0.02)
AT-02	2.34 (0.30)	783	16	43.3 (1.7)	125 ± 15	0.00	44	12.78	100	1.54	0.06 (0.02)
AT-03	2.98 (0.12)	701	15	86.3 (1.9)	68 ± 3	0.05	12	13.13	89	1.39	0.23 (0.03)
AT-04	1.73 (0.15)	899	18	44.9 (1.3)	73 ± 6	0.00	28	13.40	74	1.02	0.11 (0.03)
AT-08	0.28 (0.08)	37	6	5.78 (0.23)	132 ± 22	0.32	0.0	12.64	42*	1.26	0.06 (0.02)
AT-09	0.93 (0.09)	38	4	29.2 (0.7)	60 ± 10	0.95	0.0	12.55	40*	1.05	0.10 (0.02)
AT-10	0.77 (0.13)	89	7	9.59 (0.48)	155 ± 17	0.50	0.0	–	–	–	0.07 (0.02)
AT-11	0.97 (0.11)	236	14	13.8 (0.6)	157 ± 20	0.00	39	12.70	20*	1.26	0.05 (0.02)
AT-13	1.50 (0.26)	341	15	34.0 (1.1)	88 ± 10	0.00	40	13.66	85	1.12	0.06 (0.02)
AT-14	0.57 (0.06)	143	11	10.1 (0.4)	121 ± 11	0.24	13	–	–	–	0.05 (0.02)
AT-15	2.61 (0.27)	550	12	74.1 (1.7)	73 ± 8	0.00	37	13.24	107	1.1	0.05 (0.02)
AT-16	0.48 (0.08)	59	9	13.0 (0.5)	77 ± 13	0.09	31	13.62	21*	1.19	0.04 (0.02)
AT-17	0.38 (0.03)	125	15	8.32 (0.36)	89 ± 8	0.68	4	13.89	32*	0.77	0.05 (0.01)
AT-18	1.11 (0.12)	222	9	28.9 (1.00)	77 ± 7	0.05	18	13.52	31*	1.19	0.04 (0.02)
AT-19	1.25 (0.21)	235	9	30.9 (0.9)	75 ± 7	0.06	18	13.55	100	0.93	0.04 (0.02)

Note. ρ_s is AFT density in 10^6 tracks/cm^2, Ns is number of fission tracks counted, N is number of counted grains, ^{238}U is the average concentration of ^{238}Uranium in ppm, Central Age is the AFT central age in Ma and its 1σ uncertainty, P(χ2) is the statistical probability that the single grain ages constitute a single population (if >0.05). Disp. Is the percentage of dispersion of the single grain age distribution, l_m is the average confined AFT length in μm, n is the number of measured confined tracks (* marks samples that received ^{252}Cf irradiation), σ_c is the standard deviation of the confined track length distribution, Cl is the Chlorine concentration in weight percentage. All values in round brackets contain the uncertainties on the average values (standard error of the mean).

(Burtner et al., 1994; Donelick, 1993). Samples that fail the chi-squared test generally exhibit high U concentrations, which have been noted by McDannell (2020) to return inappropriately low chi-squared values due to the high precision obtained using the LA–ICP–MS method. The exceptions are lower U samples AT-11 and AT-02. AT-11 produced the oldest AFT central age for the study area, where AFT ages for low-U apatites cluster at ∼250 Ma (i.e., identical to the ZUPb and AUPb dates for the sample) and high-U apatites cluster around ∼100 Ma, in line with most other central ages for the study area. A similar, although less clear, trend can be observed for sample AT-02. However, more diagnostically, the youngest AFT central ages tend to correlate with proximity to major structures and locations near the Keketuohai mining area (Figure 2). Fission track length distributions are variable depending on the sample location. In general, samples that produced older (>120 Ma) AFT ages (AT-01, 02, 08, 10, 11) are characterized by broader distributions and lower mean track lengths (<13 μm). Such distributions are generally characteristic of protracted, slow cooling histories. Samples with younger (∼90–70 Ma) AFT central ages (AT-03, 04, 09, 13, 15–19) are associated with longer mean track lengths (>13 μm) and generally narrower distributions, suggesting that they record a more rapid thermal event. Sample AT-09 is the exception and records the youngest AFT central age, associated with a mean track length of ∼12.6 μm.

The "expected" QTQt thermal history model outputs are presented in Supporting Information S1 and summarized in Figure 4. Models that are based on less than 50 confined fission tracks are indicated by dashed lines and should only be considered in combination with other models that are based on more length data. The models are grouped (color code in Figure 4) according to the geographical location of the samples: (a) to the west of the Fuyun Fault (blue models), (b) to the east of the Fuyun Fault (orange paths); and (c) along major thrust faults parallel to the Irtysh Shear Zone (red paths). The models to the west of the Fuyun Fault (away from thrusts) show protracted slow cooling through the APAZ between ∼210 Ma and ∼80 Ma. The models to the east of the Fuyun Fault (Keketuohai area, Figure 2) reveal fast cooling through the APAZ between ∼100 and 75 Ma. The models for samples along thrust faults within the Irtysh Shear Zone (Figure 2) display the youngest but variable thermal histories. The majority of samples in this group enter the APAZ at ∼75 Ma followed by either fast cooling through the APAZ (AT-04 and AT-15) or an initial phase of fast cooling, followed by more protracted cooling with an

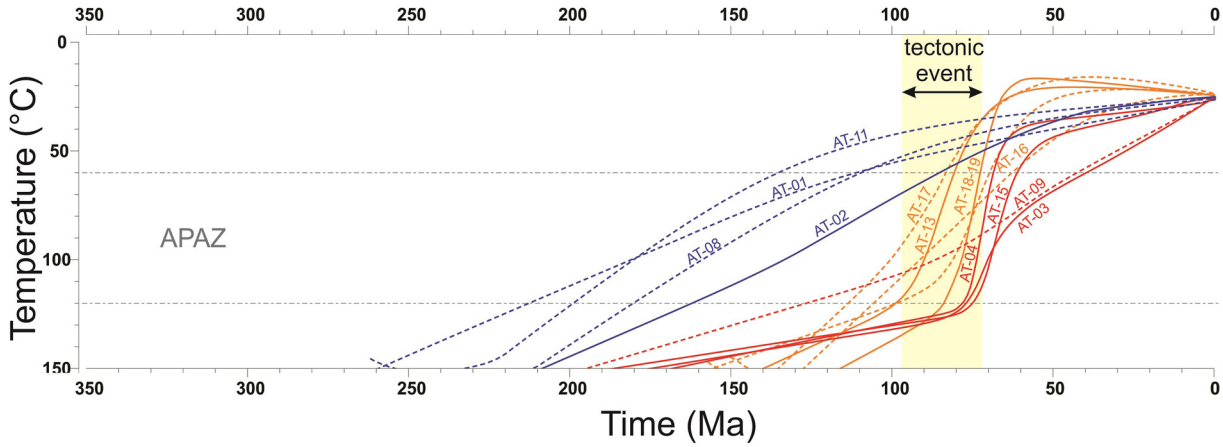

Figure 4. Summary of the "expected" QTQt thermal history models for this study. Red models correspond to samples taken in close vicinity to WNW-ESE striking thrust faults and show the youngest thermal histories of the study area. Orange models group samples taken to the NE of the Fuyun Fault, which show consistent thermal histories with rapid Late Cretaceous cooling. The blue models represent the thermal histories at lower relief and away from major structures. Dashed models are based on less than 50 confined fission track lengths and should therefore only be taken into consideration with other models from the same group. Detailed models can be accessed in Supporting Information S1.

exit out of the APAZ at ~40 Ma (AT-03). The model for AT-09 is poorly constrained and shows more protracted cooling that correlates with the model for AT-03 in the upper APAZ.

In summary, the AFT data reveal evidence for rapid cooling at ~100–75 Ma for samples taken to the northeast of the Fuyun Fault. In clear contrast is the obtained protracted slow cooling history to the west of the Fuyun Fault and away from major thrust faults, which suggests that the Fuyun Fault facilitated differential exhumation during the Late Cretaceous. Samples taken along WNW-ESE striking thrust faults in the Irtysh Shear Zone have broader length distributions and display more complex thermal histories with partial preservation of middle to Late Cretaceous cooling and subtle evidence for a subsequent younger thermal event.

6. Discussion

6.1. Late Permian Metamorphism and Middle–Late Jurassic High-Temperature Metasomatism

The Chinese Altai has been strongly deformed on multiple occasions throughout its history. The metamorphic history recorded in the Irtysh Shear Zone has been well documented by previous studies (Briggs et al., 2007, 2009; Li, Sun, et al., 2015; Li, Yuan, et al., 2015), revealing a record of Permian–Triassic metamorphism and deformation. Here, we use the apatite record to expand our understanding of the deformation history. Abundant late Permian (~260 Ma) and Middle–Late Jurassic (~170–160 Ma) AUPb ages were obtained which are younger than the corresponding zircon ages (Figure 3a). Trace element data further indicate that these apatites do not record primary igneous compositions but rather recrystallized during metamorphism or grew in an associated fluid, where other phases were competing for LREEs (e.g., Glorie, Jepson, et al., 2019). The youngest AUPb ages are of particular interest as they were obtained in close vicinity to the Keketuohai mineralized area (mined for Au-Cu-Pb-Zn-rare metals) (Liu et al., 2014; Xue et al., 2016; Zheng et al., 2017). The youngest widespread igneous rocks in this area are mostly pegmatites associated with the Alear granite and are dated by ZUPb to be ~212–210 Ma old (Table 1), consistent with previous constraints (Liu & Han, 2019). However, the sampled Devonian, Permian and Late Triassic granites in the Keketuohai area show a record of resetting to an AUPb minimum age of ~170–160 Ma (Figure 3), which corresponds to the timing of hydrothermal activity (Zhou et al., 2015).

In more detail, the trace element geochemistry for the samples with the youngest (<180 Ma) AUPb ages in this study correspond closely to those recording post-orogenic fluid alteration in the Uzbek Tian Shan (dotted outlined field in Figure 3c, based on data from Glorie, Jepson, et al. (2019), displayed in Supporting Information S1). Furthermore, the primitive-mantle normalized La/Sm versus Ce/Yb plot shows that the trace-element geochemical signatures for the <180 Ma apatite samples in this study are comparable to those for apatite samples from orogenic Au deposits in British Columbia (dotted outlined field in Figure 3d, based on data from Mao et al. (2016)). Hence, we suggest the ~170–160 Ma apatite ages record a metasomatic event that affected the Keketuohai mineralized area.

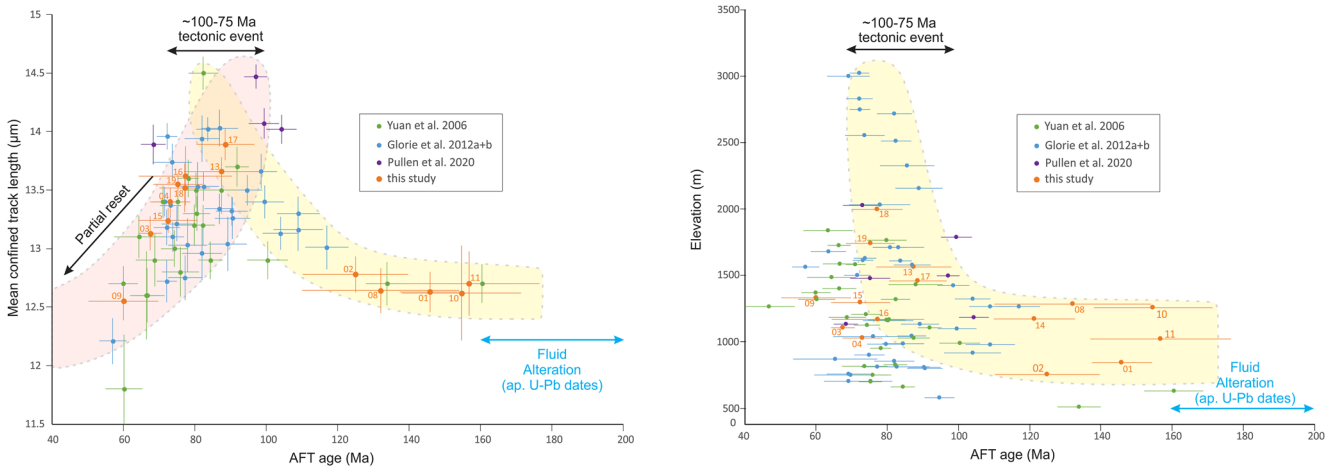

Figure 5. (a) Mean confined AFT length versus AFT age "boomerang" plot (cfr. Gallagher et al., 1998; Green et al., 1986), revealing that the ~100–75 Ma AFT ages correspond to >13.5 µm mean track lengths, indicative of a rapid cooling event. (b) AFT age versus elevation plot, revealing that samples at the highest elevations only record ~100–75 Ma cooling ages. Numbered symbols in both plots correspond to data from this study (with the numbers referring to the sample numbers). Other data were taken from Glorie, De Grave, Buslov, et al. (2012), Glorie, De Grave, Delvaux, et al. (2012), Pullen et al. (2020), and Yuan et al. (2006).

In support of this interpretation, Zhou et al. (2015) report ZUPb ages of ~175–172 Ma for the "No. 3 pegmatite" in the Keketuohai area, which are interpreted as the timing of the final hydrothermal stage of the deposit. This interpreted metasomatic event is synchronous with widespread Triassic–Jurassic anorogenic magmatism within the Altai (Liu & Han, 2019; Wang et al., 2014), including Early–Middle Jurassic (~195–172 Ma) Li and rare metal bearing pegmatites in the Keketuohai area (Zhou et al., 2015). While the fluid source of this metasomatic event is yet to be fully established, magmatic fluids associated with Triassic–Jurassic intrusions in the Altai provide a plausible origin of metasomatizing fluids.

Briggs et al. (2009) reported a range of K-feldspar and mica Ar-Ar ages for the Fuyun area, spanning between the late Permian to Early Cretaceous (~150–140 Ma). These are interpreted as indicative of a prolonged period of cooling associated with regional exhumation. The <160 Ma cooling ages were interpreted in the context of a contractional reactivation event. Of particular interest is the reported biotite Ar-Ar weighted mean age of ~156 Ma near the Keketuohai mineralized area, on the east side of the Fuyun Fault, which corresponds within uncertainty to our youngest AUPb age for this area. Hence, the reported ~160–140 Ma Ar-Ar ages in Briggs et al. (2009) could be interpreted as cooling ages after metasomatism.

6.2. Late Cretaceous Exhumation of the Chinese Altai

Following a period of Middle–Late Jurassic fluid alteration, apatite fission track data suggest that the Fuyun area underwent rapid cooling during the mid-to Late Cretaceous (~100–75 Ma). Figure 5 presents an apatite fission track age versus mean length "boomerang plot" (cfr. Gallagher et al., 1998; Green et al., 1986), which aims to interpret the significance of the newly obtained AFT data in a more regional context for the Chinese Altai. Commonly, samples yielding shorter (<13.5 µm) mean track lengths are indicative of extensive residence with in the APAZ, while samples with long track lengths have moved through the APAZ more rapidly, often due to a tectonic influence. Here, we plot our data versus a compilation of available AFT data for the Chinese Altai using results from Glorie, De Grave, Buslov, et al. (2012), Glorie, De Grave, Delvaux, et al. (2012), Pullen et al. (2020), and Yuan et al. (2006). The resulting plot shows a systematic trend for all study areas, indicating a significant rapid cooling event at ~100–75 Ma, consistent with thermal history models. In more detail, samples producing AFT ages older than ~100 Ma are associated with relatively short (<13.5 µm) mean track lengths and represent largely mixed APAZ AFT ages that span between the timing of interpreted Middle–Late Jurassic fluid alteration and a tectonic event that induced rapid cooling since ~100 Ma. In addition, the samples from this study as well as other studies in the Chinese Altai reveal a secondary trend of decreasing mean track length values with decreasing age since ~90 Ma. Samples with AFT ages younger than ~75 Ma are again associated with lower mean track values and broader fission track distributions, suggesting that they are likely partially reset by a younger, Cenozoic event. However, the available data cannot constrain the timing of this younger event. Hence, the <75 Ma AFT ages are

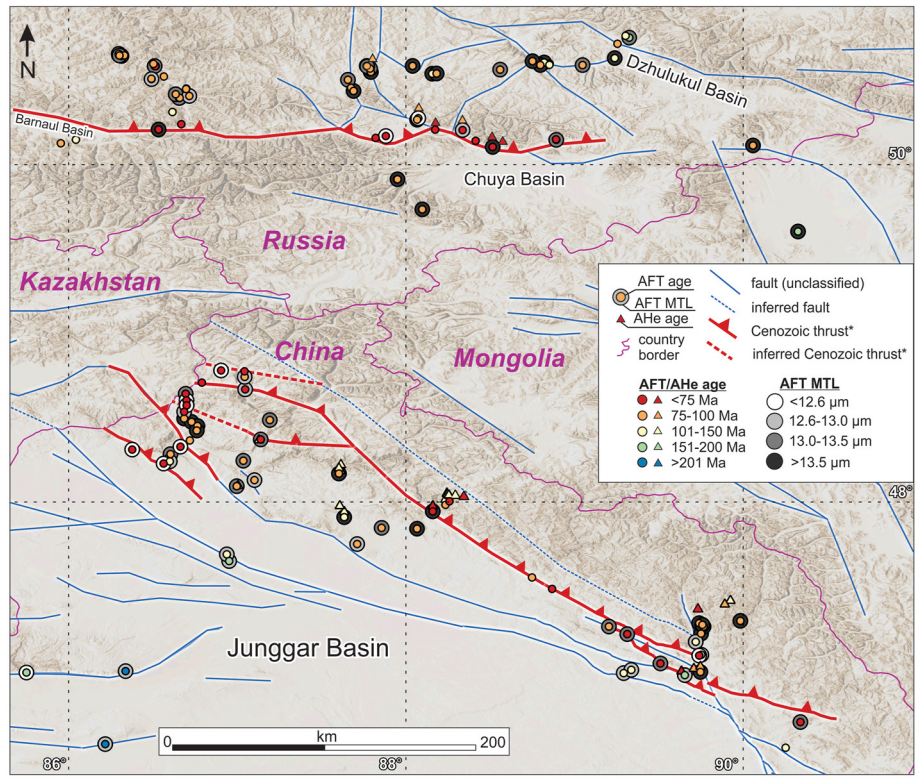

Figure 6. Digital elevation model for the Altai with indication of AFT samples from this study and published studies (De Grave et al., 2008; Glorie, De Grave, Buslov, et al., 2012; Pullen et al., 2020; Yuan et al., 2006). Samples are color-coded as in Figure 2. Major faults are displayed following structural maps from Yuan et al. (2006), Cunningham (2007), Glorie, De Grave, Buslov, et al. (2012), Li, Sun, et al. (2015) and references therein. The inferred faults in the northwestern Chinese Tian Shan were drawn after Liu et al. (2012). *Thrust faults displayed in red are interpreted to be reactivated during the Cenozoic based on the AFT data (<75 Ma AFT age and reduced MTL values; see text for further explanations).

interpreted as mixed apparent ages that record partial preservation of the ~100–75 Ma cooling event and the influence of a younger event that has only marginally affected the samples at the present-day surface. The age-elevation plot (cfr. Naeser, 1976; Wagner & Reimer, 1972) reveals a similar trend (Figure 5). At low elevations (<1,500 m), a range of apparent AFT ages can be observed, reflective of slow cooling. Notably, at higher elevations (>1,500 m), the AFT ages are exclusively ~100–75 Ma, indicative of a rapid cooling event. As these rapid Late Cretaceous cooling ages are preserved at high altitude, this suggests that a younger, secondary event must have driven exhumation and that denudation has been limited to preserve the Late Cretaceous AFT ages. Highest elevation samples within the Altai are from the northern Chinese and Siberian Altai, while topographic relief is more moderate in the Fuyun area.

Figure 6 displays the spatial distribution of published and new AFT data (ages as symbol colors, MTL values as gray-scale rims). The ~100–75 Ma ages are indicated in orange and correspond with dark gray symbol rims (high mean track lengths) throughout the entire Altai. Younger and older AFT ages (red and yellow-green-blue symbol colors) are generally associated with lower mean track lengths (lighter gray symbol rims). Similar data can be observed in the westernmost Chinese Altai and across the entire Siberian Altai (southwest and north sections of Figure 6) in study areas away from the main structural boundaries (De Grave et al., 2008; Glorie, De Grave, Buslov, et al., 2012; Yuan et al., 2006). Hence, the Cretaceous cooling event can be regarded as a regional event that affected much of the Altai orogenic system.

In the Fuyun area, contrasting AFT data are evident for either side of the Fuyun Fault (Figure 2). In more detail, samples taken to the east of the Fuyun Fault, record rapid early Late Cretaceous exhumation (orange symbols with dark rim), while samples to the west, away from WNW-ESE striking faults associated with the Irtysh Shear Zone record slowly cooled Late Jurassic–Early Cretaceous thermal histories (yellow-green symbols with light gray rim). The differential nature of the AFT ages and cooling histories with respect to the Fuyun Fault suggests

that the Fuyun Fault was active during the Late Cretaceous. As a consequence of this differential uplift, topography preserved to the east of the Fuyun Fault is notably higher than observed in the west (Table 1; Figure 2). These data therefore suggests that strain associated with the Late Cretaceous tectonic event that induced regional exhumation in the Altai was largely accommodated by the Fuyun Fault in the Fuyun area, rather than the Irtysh Shear Zone. This is in contrast to the Kazakh Altai to the west, where samples taken in close vicinity to the Irtysh Shear Zone record a fast early Late Cretaceous cooling pulse (~100–80 Ma; Glorie, De Grave, Delvaux, et al., 2012), suggesting some heterogeneity of reactivation along the Irtysh Shear Zone within the broader Altai.

The timing of formation of the Fuyun Fault itself is not well understood. Lin (1994) observed that the fault displaces (unspecified) granite intrusions of ~110–80 Ma in age, and therefore suggested that the Fuyun Fault must be younger than ~110–80 Ma, although the credibility of these granite dates is difficult to assess without detailed sample location information. These granitic intrusion ages are, however, consistent with low-temperature thermochronological data presented in this study, which suggest movement of the Fuyun Fault in the Late Cretaceous, and help define the minimum formation age of this structure. Detailed age constraints on Mesozoic structures within the Fuyun area are presently scarce, so it is unclear whether the Fuyun Fault formed during the Cretaceous or if observed differential uplift reflects the reactivation of a pre-existing structure.

The sedimentary history of the adjacent Junggar Basin suggests that the Late Cretaceous exhumation can be linked to a period of significant exhumation and denudation. The Junggar Basin accumulated >5 km of terrestrial sediments during the Mesozoic, including debris flows, alluvial fans, braided rivers and lacustrine deposits (Wang & Chen, 2004). Additionally, the Ob-Zaisan Basin (Figure 1), which is associated with the Irtysh Shear Zone to the west of the Fuyun area, records ~6 km of Meso-Cenozoic clastic sediment that have been linked to the adjacent eroding Altai orogeny (Thomas et al., 2002). Late Cretaceous exhumation is coeval with a number of far-field tectonic events, however, the precise cause of reactivation within the Altai is debated. Exhumation is contemporaneous with both collapse of the Mongol-Okhotsk Orogen, to the east of the study area (Jolivet et al., 2009; Metelkin et al., 2012), and slab rollback in the Tethys Ocean to the south at ~100–80 Ma (Dilek & Furnes, 2009; Glorie, Otasevic, et al., 2019; Ma et al., 2013; Yin et al., 2019), both of which are plausible drivers of propagation of stress to the continental interior and consequential reactivation and exhumation. It is, however, unclear from current data the extent to which these events impacted reactivation within the Altai.

6.3. Cenozoic Reactivation in the Altai

As discussed above, the age versus mean track length plot (Figure 5) predicts that some samples record partial reset of the AFT clock, after the Late Cretaceous. Figure 6 reveals that these samples correspond to locations along the main E-W and SE-NW frontal thrust systems in both the Chinese and Siberian Altai (indicated in red on Figure 6). In more detail, the combined data-set dates Cenozoic activity along mapped thrust faults within the Irtysh Shear Zone (and inferred equivalents based on topographic continuations) as well as thrusts to the south at the very edge of the Junggar Basin, where the Altai is overriding the Junggar margin (Figure 6). Within Siberia, the data predicts that the fault system that runs from the Barnaul Basin to the Chuya Basin (which records recent seismic activity in places (e.g., Novikov et al., 2008)) was active in the Cenozoic as well. These faults are structures that formed during the amalgamation of the Central Asian Orogenic Belt that were reactivated during the far-field effects of Cenozoic distal tectonic events (De Grave et al., 2007; Glorie & De Grave, 2016). While the presented AFT data do not allow for resolution of the timing of Cenozoic fault displacement, the data set provides evidence for partial resetting along those faults. We suggest that the Cenozoic thrusts induced associated exhumation to a level where the Cretaceous cooling signal is now preserved in the highest peaks of the Altai, but where the Cenozoic imprint has not made it to the present-day surface. This can be explained by a scenario where denudation has not caught up with exhumation as typically observed in recent thrust systems (e.g., Glorie & De Grave, 2016; Jolivet, 2017) and relatively arid landscapes (e.g., Charreau et al., 2017; Pullen et al., 2020). In absence of other testable alternatives, we speculate that the driver for Cenozoic reactivation is related to the far-field India-Eurasia collision, similar as discussed in previous literature (De Grave et al., 2007; Glorie, De Grave, Buslov, et al., 2012).

7. Conclusions

Based on the apatite U-Pb, fission track and trace element geochemistry results from this study, in combination with previous studies, the following conclusions can be made for the Mesozoic–Cenozoic thermal history of the Altai:

1. Following granite emplacement during the Triassic, the Fuyun area records a period of metasomatism during the Jurassic. The youngest apatite U-Pb dates in this study (~170–160 Ma) are preserved in the Keketuohai area and correspond with the timing of the hydrothermal stage of pegmatitic rare-metal mineralization.
2. More regionally, the Jurassic is characterized by slow low-temperature cooling rates, as preserved in the thermal history profiles in low-relief areas of the Altai.
3. Areas with more significant relief record a regional pulse of early Late Cretaceous (~100–75 Ma) rapid cooling throughout the Altai. This cooling event corresponds with km-scale deposition of coarse sediments in adjacent basins, such as the Junggar Basin, and is therefore interpreted as a regional event of exhumation and denudation-driven cooling. The tectonic driver responsible for this cooling pulse is debated, but may be linked to the collapse of the Mongol-Okhotsk Orogen to the east, or to extensional tectonics related with slab-rollback in the distant Tethys Ocean to the south.
4. Samples taken near the frontal thrusts of the Altai show evidence for partial resetting of the fission track clock during the Cenozoic. However, since denudation has not caught up with exhumation along these structures, the timing of this Cenozoic reactivation event cannot be determined using outcrop samples.

Data Availability Statement

Original data generated from this study are openly available on the Figshare database (Supporting Information S2 https://doi.org/10.25909/21590265; Supporting Information S3 https://doi.org/10.25909/21590286; Supporting Information S4 https://doi.org/10.25909/21590292; Supporting Information S5 https://doi.org/10.25909/21590310).

Acknowledgments
This paper was supported by research Grants DP150101730 and DP200101881 from the Australian Research Council. Sarah Gilbert is thanked for technical assistance with the analytical facilities at Adelaide Microscopy. Open access publishing facilitated by The University of Adelaide, as part of the Wiley - The University of Adelaide agreement via the Council of Australian University Librarians.

References

Briggs, S. M., Yin, A., Manning, C. E., Chen, Z.-L., & Wang, X.-F. (2009). Tectonic development of the southern Chinese Altai Range as determined by structural geology, thermobarometry, $^{40}Ar/^{39}Ar$ thermochronology, and Th/Pb ion-microprobe monazite geochronology. *GSA Bulletin*, *121*(9–10), 1381–1393. https://doi.org/10.1130/B26385.1

Briggs, S. M., Yin, A., Manning, C. E., Chen, Z.-L., Wang, X.-F., & Grove, M. (2007). Late Paleozoic tectonic history of the Ertix Fault in the Chinese Altai and its implications for the development of the Central Asian Orogenic System. *Geological Society of America Bulletin*, *119*(7–8), 944–960. https://doi.org/10.1130/B26044.1

Burtner, R. L., Nigrini, A., & Donelick, R. A. (1994). Thermochronology of lower cretaceous source rocks in the Idaho-Wyoming thrust belt. *AAPG Bulletin*, *78*(10), 1613–1636. https://doi.org/10.1306/a25ff233-171b-11d7-8645000102c1865d

Buslov, M., Watanabe, T., Fujiwara, Y., Iwata, K., Smirnova, L., Safonova, I. Y., et al. (2004). Late Paleozoic faults of the Altai region, Central Asia: Tectonic pattern and model of formation. *Journal of Asian Earth Sciences*, *23*(5), 655–671. https://doi.org/10.1016/S1367-9120(03)00131-7

Buslov, M. M., Geng, H., Travin, A. V., Otgonbaatar, D., Kulikova, A. V., Ming, C., et al. (2013). Tectonics and geodynamics of Gorny Altai and adjacent structures of the Altai–Sayan folded area. *Russian Geology and Geophysics*, *54*(10), 1250–1271. https://doi.org/10.1016/j.rgg.2013.09.009

Buslov, M. M., Safonova, I. Y., Watanabe, N., Obut, O. T., Fujiwara, I., Iwata, K., et al. (2001). Evolution of the Palaeo-Asian ocean (Altai-Sayan region, central Asia) and collision of possible Gondwana-derived terranes with the southern marginal part of the Siberian continent. *Geosciences Journal*, *5*(3), 203–204. https://doi.org/10.1007/BF02910304

Chang, E. Z., Coleman, R. G., & Ying, D. X. (1995). *Tectonic transect map across Russia-Mongolia-China*. Stanford University Press.

Chen, B., & Jahn, B.-M. (2002). Geochemical and isotopic studies of the sedimentary and granitic rocks of the Altai orogen of northwest China and their tectonic implications. *Geological Magazine*, *139*(1), 1–13. https://doi.org/10.1017/s0016756801006100

Charreau, J., Saint-Carlier, D., Dominguez, S., Lavé, J., Blard, P.-H., Avouac, J.-P., et al. (2017). Denudation outpaced by crustal thickening in the eastern Tianshan. *Earth and Planetary Science Letters*, *479*, 179–191. https://doi.org/10.1016/j.epsl.2017.09.025

Cherniak, D. J. (2010). Diffusion in accessory minerals: Zircon, Titanite, apatite, monazite and Xenotime. *Reviews in Mineralogy and Geochemistry*, *72*(1), 827–869. https://doi.org/10.2138/rmg.2010.72.18

Chew, D. M., Petrus, J. A., & Kamber, B. S. (2014). U-Pb LA-ICPMS dating using accessory mineral standards with variable common Pb. *Chemical Geology*, *363*, 185–199. https://doi.org/10.1016/j.chemgeo.2013.11.006

Cunningham, D. (2007). Structural and topographic characteristics of restraining bend mountain ranges of the Altai, Gobi Altai and easternmost Tien Shan. *Geological Society, London, Special Publications*, *290*(1), 219–237. https://doi.org/10.1144/SP290.7

Cunningham, D., Dijkstra, A., Howard, J., Quarles, A., & Badarch, G. (2003). *Active intraplate strike-slip faulting and transpressional uplift in the Mongolian Altai* (Vol. 210, pp. 65–87). Geological Society, London, Special Publications. https://doi.org/10.1144/GSL.SP.2003.210.01.05

De Grave, J., Buslov, M. M., & Van den haute, P. (2007). Distant effects of India–Eurasia convergence and Mesozoic intracontinental deformation in Central Asia: Constraints from apatite fission-track thermochronology. *Journal of Asian Earth Sciences*, *29*(2–3), 188–204. https://doi.org/10.1016/j.jseaes.2006.03.001

De Grave, J., Buslov, M. M., Van Den Haute, P., Metcalf, J., Dehandschutter, B., & McWilliams, M. O. (2009). Multi-method chronometry of the Teletskoye graben and its basement, Siberian Altai mountains: New insights on its thermo-tectonic evolution. *Geological Society, London, Special Publications*, *324*(1), 237–259. https://doi.org/10.1144/SP324.17

De Grave, J., De Pelsmaeker, E., Zhimulev, F. I., Glorie, S., Buslov, M. M., & Van den haute, P. (2014). Meso-Cenozoic building of the northern central Asian orogenic belt: Thermotectonic history of the Tuva region. *Tectonophysics*, *621*, 44–59. https://doi.org/10.1016/j.tecto.2014.01.039

De Grave, J., Glorie, S., Buslov, M. M., Stockli, D. F., McWilliams, M. O., Batalev, V. Y., & Van den haute, P. (2013). Thermo-tectonic history of the Issyk-Kul basement (Kyrgyz northern Tien Shan, central Asia). *Gondwana Research*, *23*(3), 998–1020. https://doi.org/10.1016/j.gr.2012.06.014

De Grave, J., & Van den haute, P. (2002). Denudation and cooling of the Lake Teletskoye Region in the Altai Mountains (South Siberia) as revealed by apatite fission-track thermochronology. *Tectonophysics*, *349*(1-4), 145–159. https://doi.org/10.1016/S0040-1951(02)00051-3

De Grave, J., Van den Haute, P., Buslov, M. M., Dehandschutter, B., & Glorie, S. (2008). Apatite fission-track thermochronology applied to the Chulyshman plateau, Siberian Altai region. *Radiation Measurements*, *43*(1), 38–42. https://doi.org/10.1016/j.radmeas.2007.11.068

De Pelsmaeker, E., Glorie, S., Buslov, M. M., Zhimulev, F. I., Poujol, M., Korobkin, V. V., et al. (2015). Late-Paleozoic emplacement and Meso-Cenozoic reactivation of the southern Kazakhstan granitoid basement. *Tectonophysics*, *662*, 416–433. https://doi.org/10.1016/j.tecto.2015.06.014

Dilek, Y., & Furnes, H. (2009). Structure and geochemistry of Tethyan ophiolites and their petrogenesis in subduction rollback systems. *Lithos*, *113*(1), 1–20. https://doi.org/10.1016/j.lithos.2009.04.022

Donelick, R. A. (1993). Apatite etching characteristics versus chemical composition. *Nuclear Tracks and Radiation Measurements*, *21*(604).

Donelick, R. A., & Miller, D. S. (1991). Enhanced tint fission track densities in low spontaneous track density apatites using 252Cf-derived fission fragment tracks: A model and experimental observations. *International Journal of Radiation Applications and Instrumentation - Part D: Nuclear Tracks and Radiation Measurements*, *18*(3), 301–307. https://doi.org/10.1016/1359-0189(91)90022-a

Dumitru, T. A., Zhou, D., Chang, E. Z., Graham, S. A., Hendrix, M. S., Sobel, E. R., & Carroll, A. R. (2001). *Uplift, exhumation, and deformation in the Chinese Tian Shan* (Vol. 194, pp. 71–99). Geological Society of America Memoirs.

Fernie, N., Glorie, S., Jessell, M. W., & Collins, A. S. (2018). Thermochronological insights into reactivation of a continental shear zone in response to Equatorial Atlantic rifting (northern Ghana). *Scientific Reports*, *8*(1), 16619. https://doi.org/10.1038/s41598-018-34769-x

Flowers, R. M., Farley, K. A., & Ketcham, R. A. (2015). A reporting protocol for thermochronologic modeling illustrated with data from the Grand Canyon. *Earth and Planetary Science Letters*, *432*, 425–435. https://doi.org/10.1016/j.epsl.2015.09.053

Gallagher, K. (2012). Transdimensional inverse thermal history modeling for quantitative thermochronology. *Journal of Geophysical Research*, *117*(B2), B02408. https://doi.org/10.1029/2011jb008825

Gallagher, K., Brown, R., & Johnson, C. (1998). Fission track analysis and its applications to geological problems. *Annual Review of Earth and Planetary Sciences*, *26*(1), 519–572. https://doi.org/10.1146/annurev.earth.26.1.519

Gillespie, J., Glorie, S., Jepson, G., Xiao, W., & Collins, A. S. (2020). Late Paleozoic exhumation of the West Junggar mountains, NW China. *Journal of Geophysical Research: Solid Earth*, *125*(1), e2019JB018013. https://doi.org/10.1029/2019JB018013

Gillespie, J., Glorie, S., Jepson, G., Zhang, Z. Y., Xiao, W. J., Danišík, M., & Collins, A. S. (2017). Differential exhumation and crustal tilting in the easternmost Tianshan (Xinjiang, China), revealed by low-temperature thermochronology. *Tectonics*, *36*(10), 2142–2158. https://doi.org/10.1002/2017TC004574

Gillespie, J., Glorie, S., Jepson, G., Zhimulev, F., Gurevich, D., Danisik, M., & Collins, A. S. (2021). Inherited structure as a control on late Paleozoic and Mesozoic exhumation of the Tarbagatai Mountains, southeastern Kazakhstan. *Journal of the Geological Society*, *178*(6). https://doi.org/10.1144/jgs2020-121

Gillespie, J., Glorie, S., Khudoley, A., & Collins, A. S. (2018). Detrital apatite U-Pb and trace element analysis as a provenance tool: Insights from the Yenisey Ridge (Siberia). *Lithos*, *314–315*, 140–155. https://doi.org/10.1016/j.lithos.2018.05.026

Gillespie, J., Glorie, S., Xiao, W., Zhang, Z., Collins, A. S., Evans, N., et al. (2017). Mesozoic reactivation of the Beishan, southern central Asian orogenic belt: Insights from low-temperature thermochronology. *Gondwana Research*, *43*, 107–122. https://doi.org/10.1016/j.gr.2015.10.004

Glorie, S., Alexandrov, I., Nixon, A., Jepson, G., Gillespie, J., & Jahn, B. M. (2017). Thermal and exhumation history of Sakhalin Island (Russia) constrained by apatite U-Pb and fission track thermochronology. *Journal of Asian Earth Sciences*, *143*, 326–342. https://doi.org/10.1016/j.jseaes.2017.05.011

Glorie, S., & De Grave, J. (2016). Exhuming the Meso-Cenozoic Kyrgyz Tianshan and Siberian Altai-Sayan: A review based on low-temperature thermochronology. *Geoscience Frontiers*, *7*(2), 155–170. https://doi.org/10.1016/j.gsf.2015.04.003

Glorie, S., De Grave, J., Buslov, M. M., Elburg, M. A., Stockli, D. F., Gerdes, A., & Van den haute, P. (2010). Multi-method chronometric constraints on the evolution of the Northern Kyrgyz Tien Shan granitoids (Central Asian Orogenic Belt): From emplacement to exhumation. *Journal of Asian Earth Sciences*, *38*(3), 131–146. https://doi.org/10.1016/j.jseaes.2009.12.009

Glorie, S., De Grave, J., Buslov, M. M., Zhimulev, F. I., Elburg, M. A., & Van den haute, P. (2012). Structural control on Meso-Cenozoic tectonic reactivation and denudation in the Siberian Altai: Insights from multi-method thermochronometry. *Tectonophysics*, *544–545*, 75–92. https://doi.org/10.1016/j.tecto.2012.03.035

Glorie, S., De Grave, J., Buslov, M. M., Zhimulev, F. I., Izmer, A., Vandoorne, W., et al. (2011). Formation and Paleozoic evolution of the Gorny-Altai–Altai-Mongolia suture zone (south Siberia): Zircon U/Pb constraints on the igneous record. *Gondwana Research*, *20*(2), 465–484. https://doi.org/10.1016/j.gr.2011.03.003

Glorie, S., De Grave, J., Buslov, M. M., Zhimulev, F. I., Stockli, D. F., Batalev, V. Y., et al. (2011). Tectonic history of the Kyrgyz South Tien Shan (Atbashi-Inylchek) suture zone: The role of inherited structures during deformation-propagation. *Tectonics*, *30*(6), TC6016. https://doi.org/10.1029/2011TC002949

Glorie, S., De Grave, J., Delvaux, D., Buslov, M. M., Zhimulev, F. I., Vanhaecke, F., et al. (2012). Tectonic history of the Irtysh shear zone (NE Kazakhstan): New constraints from zircon U/Pb dating, apatite fission track dating and palaeostress analysis. *Journal of Asian Earth Sciences*, *45*, 138–149. https://doi.org/10.1016/j.jseaes.2011.09.024

Glorie, S., Jepson, G., Konopelko, D., Mirkamalov, R., Meeuws, F., Gilbert, S., et al. (2019). Thermochronological and geochemical footprints of post-orogenic fluid alteration recorded in apatite: Implications for mineralization in the Uzbek Tian Shan. *Gondwana Research*, *71*, 1–15. https://doi.org/10.1016/j.gr.2019.01.011

Glorie, S., March, S., Nixon, A., Meeuws, F., O'Sullivan, G. J., Chew, D. M., et al. (2020). Apatite U–Pb dating and geochemistry of the Kyrgyz South Tian Shan (Central Asia): Establishing an apatite fingerprint for provenance studies. *Geoscience Frontiers*, *11*(6), 2003–2015. https://doi.org/10.1016/j.gsf.2020.06.003

Glorie, S., Otasevic, A., Gillespie, J., Jepson, G., Danišík, M., Zhimulev, F. I., et al. (2019). Thermo-tectonic history of the Junggar Alatau within the central Asian orogenic belt (SE Kazakhstan, NW China): Insights from integrated apatite U/Pb, fission track and (U–Th)/He thermochronology. *Geoscience Frontiers*, *10*(6), 2153–2166. https://doi.org/10.1016/j.gsf.2019.05.005

Green, P. F., Duddy, I. R., Gleadow, A. J. W., Tingate, P. R., & Laslett, G. M. (1986). Thermal annealing of fission tracks in apatite: 1. A qualitative description. *Chemical Geology*, *59*, 237–253. https://doi.org/10.1016/0168-9622(86)90074-6

Hasebe, N., Tamura, A., & Arai, S. (2013). Zeta equivalent fission-track dating using LA-ICP-MS and examples with simultaneous U–Pb dating. *Island Arc*, *22*(3), 280–291. https://doi.org/10.1111/iar.12040

Hendrix, M. S., Dumitru, T. A., & Graham, S. A. (1994). Late Oligocene-early Miocene unroofing in the Chinese Tian Shan: An early effect of the India-Asia collision. *Geology*, *22*(6), 487–490. https://doi.org/10.1130/0091-7613(1994)022<0487:Loemui>2.3.Co;2

Hendrix, M. S., Graham, S. A., Carroll, A. R., Sobel, E. R., McKnight, C. L., Schulein, B. J., & Wang, Z. (1992). Sedimentary record and climatic implications of recurrent deformation in the Tian Shan: Evidence from Mesozoic strata of the north Tarim, south Junggar, and Turpan basins, northwest China. *GSA Bulletin*, *104*(1), 53–79. https://doi.org/10.1130/0016-7606(1992)104<0053:Sracio>2.3.Co;2

Hu, W., Li, P., Rosenbaum, G., Liu, J., Jourdan, F., Jiang, Y., et al. (2020). Structural evolution of the eastern segment of the Irtysh shear zone: Implications for the collision between the east Junggar Terrane and the Chinese Altai orogen (northwestern China). *Journal of Structural Geology*, *139*, 104126. https://doi.org/10.1016/j.jsg.2020.104126

Jackson, S. E., Pearson, N. J., Griffin, W. L., & Belousova, E. A. (2004). The application of laser ablation-inductively coupled plasma-mass spectrometry to in situ U–Pb zircon geochronology. *Chemical Geology*, *211*(1–2), 47–69. https://doi.org/10.1016/j.chemgeo.2004.06.017

Janousek, V., Farrow, C. M., & Erban, V. (2006). Interpretation of whole-rock geochemical data in igneous geochemistry: Introducing geochemical data Toolkit (GCDkit). *Journal of Petrology*, *47*(6), 1255–1259. https://doi.org/10.1093/petrology/egl013

Jolivet, M. (2017). Mesozoic tectonic and topographic evolution of central Asia and Tibet: A preliminary synthesis. *Geological Society, London, Special Publications*, *427*(1), 19–55. https://doi.org/10.1144/SP427.2

Jolivet, M., De Boisgrollier, T., Petit, C., Fournier, M., Sankov, V. A., Ringenbach, J.-C., et al. (2009). How old is the Baikal Rift Zone? Insight from apatite fission track thermochronology. *Tectonics*, *28*(3), TC3008. https://doi.org/10.1029/2008TC002404

Jolivet, M., Dominguez, S., Charreau, J., Chen, Y., Li, Y., & Wang, Q. (2010). Mesozoic and Cenozoic tectonic history of the central Chinese Tian Shan: Reactivated tectonic structures and active deformation. *Tectonics*, *29*(6), TC6019. https://doi.org/10.1029/2010TC002712

Jolivet, M., Heilbronn, G., Robin, C., Barrier, L., Bourquin, S., Guo, Z., et al. (2013). Reconstructing the late Paleozoic—Mesozoic topographic evolution of the Chinese Tian Shan: Available data and remaining uncertainties. *Advances in Geosciences*, *37*, 7–18. https://doi.org/10.5194/adgeo-37-7-2013

Jolivet, M., Ritz, J.-F., Vassallo, R., Larroque, C., Braucher, R., Todbileg, M., et al. (2007). Mongolian summits: An uplifted, flat, old but still preserved erosion surface. *Geology*, *35*(10), 871–874. https://doi.org/10.1130/g23758a.1

Kirkland, C. L., Fougerouse, D., Reddy, S. M., Hollis, J., & Saxey, D. W. (2018). Assessing the mechanisms of common Pb incorporation into titanite. *Chemical Geology*, *483*, 558–566. https://doi.org/10.1016/j.chemgeo.2018.03.026

Laurent-Charvet, S., Charvet, J., Shu, L., Ma, R., & Lu, H. (2002). Palaeozoic late collisional strike-slip deformations in Tianshan and Altay, eastern Xinjiang, NW China. *Terra Nova*, *14*(4), 249–256. https://doi.org/10.1046/j.1365-3121.2002.00417.x

Li, A., Xu, Y., Liao, W., Han, B.-F., & Wei, C. (2022). High-pressure granulite-facies metamorphism in the junction between the Siberian and Kazakhstan-Junggar continents and implications for the assembly of Pangea. *Gondwana Research*, *110*, 13–30. https://doi.org/10.1016/j.gr.2022.06.006

Li, C., Li, Z., Zeng, M., & Stern, R. J. (2022). Early Eocene A-type (ferroan) rhyolites in southwestern Tibet: A far-field tectonic effect of the India–Eurasia collision. *International Geology Review*, 1–20. https://doi.org/10.1080/00206814.2022.2117740

Li, P., Sun, M., Rosenbaum, G., Cai, K., & Yu, Y. (2015). Structural evolution of the Irtysh shear zone (northwestern China) and implications for the amalgamation of arc systems in the central Asian orogenic belt. *Journal of Structural Geology*, *80*, 142–156. https://doi.org/10.1016/j.jsg.2015.08.008

Li, P., Sun, M., Rosenbaum, G., Jourdan, F., Li, S., & Cai, K. (2017). Late Paleozoic closure of the Ob-Zaisan Ocean along the Irtysh shear zone (NW China): Implications for arc amalgamation and oroclinal bending in the Central Asian orogenic belt. *Geological Society of America Bulletin*, *129*(5–6), 547–569. https://doi.org/10.1130/B31541.1

Li, P., Yuan, C., Sun, M., Long, X., & Cai, K. (2015). Thermochronological constraints on the late Paleozoic tectonic evolution of the southern Chinese Altai. *Journal of Asian Earth Sciences*, *113*, 51–60. https://doi.org/10.1016/j.jseaes.2014.11.004

Li, S., Wang, T., Wilde, S. A., & Tong, Y. (2013). Evolution, source and tectonic significance of Early Mesozoic granitoid magmatism in the Central Asian Orogenic Belt (central segment). *Earth-Science Reviews*, *126*, 206–234. https://doi.org/10.1016/j.earscirev.2013.06.001

Lin, A. (1994). Glassy pseudotachylyte veins from the Fuyun fault zone, northwest China. *Journal of Structural Geology*, *16*(1), 71–83. https://doi.org/10.1016/0191-8141(94)90019-1

Liu, F., & Han, D. (2019). Petrogenetic and tectonic implications of Triassic granitoids in the Chinese Altay: The Alaer granite example. *Heliyon*, *5*(2), e01261. https://doi.org/10.1016/j.heliyon.2019.e01261

Liu, F., Zhang, Z. X., Li, Q., Zhang, C., & Li, C. (2014). New precise timing constraint for the Keketuohai No. 3 pegmatite in Xinjiang, China, and identification of its parental pluton. *Ore Geoogyl Reviews*, *56*, 209–219. https://doi.org/10.1016/j.oregeorev.2013.08.020

Liu, W., Liu, X. J., & Xiao, W. J. (2012). Massive granitoid production without massive continental-crust growth in the Chinese Altay: Insight into the source rock of granitoids using integrated zircon U-Pb age, Hf-Nd-Sr isotopes and geochemistry. *American Journal of Science*, *312*(6), 629–684. https://doi.org/10.2475/06.2012.02

Lü, H. H., Chang, Y., Wang, W., & Zhou, Z. Y. (2013). Rapid exhumation of the Tianshan Mountains since the early Miocene: Evidence from combined apatite fission track and (U-Th)/He thermochronology. *Science China Earth Sciences*, *56*(12), 2116–2125. https://doi.org/10.1007/s11430-013-4715-1

Ma, L., Wang, D., Li, Z.-X., Wyman, D. A., Jiang, Z.-Q., Yang, J.-H., et al. (2013). Early Late Cretaceous (ca. 93Ma) norites and hornblendites in the Milin area, eastern Gangdese: Lithosphere–asthenosphere interaction during slab roll-back and an insight into early Late Cretaceous (ca. 100–80Ma) magmatic "flare-up" in southern Lhasa (Tibet). *Lithos*, *172–173*, 17–30. https://doi.org/10.1016/j.lithos.2013.03.007

Macaulay, E. A., Sobel, E. R., Mikolaichuk, A., Kohn, B., & Stuart, F. M. (2014). Cenozoic deformation and exhumation history of the Central Kyrgyz Tien Shan. *Tectonics*, *33*(2), 135–165. https://doi.org/10.1002/2013TC003376

Mao, M., Rukhlov, A. S., Rowins, S. M., Spence, J., & Coogan, L. A. (2016). Apatite trace element compositions: A robust new Tool for mineral Exploration. *Economic Geology*, *111*(5), 1187–1222. https://doi.org/10.2113/econgeo.111.5.1187

McDannell, K. T. (2020). Notes on statistical age dispersion in fission-track datasets: The chi-square test, annealing variability, and analytical considerations. *Down to Earth*. https://doi.org/10.31223/osf.io/uj4hx

McDannell, K. T., Zeitler, P. K., & Idleman, B. D. (2018). Relict topography within the Hangay Mountains in central Mongolia: Quantifying long-term exhumation and relief change in an old landscape. *Tectonics*, *37*(8), 2531–2558. https://doi.org/10.1029/2017TC004682

McDonough, W. F., & Sun, S. S. (1995). The composition of the Earth. *Chemical Geology*, *120*(3–4), 223–253. https://doi.org/10.1016/0009-2541(94)00140-4

McDowell, F. W., McIntosh, W. C., & Farley, K. A. (2005). A precise ^{40}Ar–^{39}Ar reference age for the Durango apatite (U–Th)/He and fission-track dating standard. *Chemical Geology*, *214*(3–4), 249–263. https://doi.org/10.1016/j.chemgeo.2004.10.002

Metelkin, D. V., Vernikovsky, V. A., & Kazansky, A. Y. (2012). Tectonic evolution of the Siberian paleocontinent from the Neoproterozoic to the late Mesozoic: Paleomagnetic record and reconstructions. *Russian Geology and Geophysics*, *53*(7), 675–688. https://doi.org/10.1016/j.rgg.2012.05.006

Mohadjer, S., Ehlers, T. A., Bendick, R., Stubner, K., & Strube, T. (2016). A Quaternary fault database for central Asia. *Natural Hazards and Earth System Sciences*, *16*(2), 529–542. https://doi.org/10.5194/nhess-16-529-2016

Mohadjer, S., Strube, T., Ehlers, T. A., & Bendick, R. (2015). Central Asia fault database. (ONLINE) (02/05/19) Retrieved from esdynamics.geo.uni-tuebingen.de/faults/

Molnar, P., & Tapponnier, P. (1975). Cenozoic tectonics of Asia: Effects of a continental collision: Features of recent continental tectonics in Asia can be interpreted as results of the India-Eurasia collision. *Science*, *189*(4201), 419–426. https://doi.org/10.1126/science.189.4201.419

Nachtergaele, S., De Pelsmaeker, E., Glorie, S., Zhimulev, F., Jolivet, M., Danišík, M., et al. (2018). Meso-Cenozoic tectonic evolution of the Talas-Fergana region of the Kyrgyz Tien Shan revealed by low-temperature basement and detrital thermochronology. *Geoscience Frontiers*, *9*(5), 1495–1514. https://doi.org/10.1016/j.gsf.2017.11.007

Naeser, C. W. (1976). Fission track dating, United States Geological Survey. *Open File Report*, *86*, 76–190.

Novikov, I. S., Emanov, A. A., Leskova, E. V., Batalev, V. Y., Rybin, A. K., & Bataleva, E. A. (2008). The system of neotectonic faults in southeastern Altai: Orientations and geometry of motion. *Russian Geology and Geophysics*, *49*(11), 859–867. https://doi.org/10.1016/j.rgg.2008.04.005

O'Sullivan, G., Chew, D., Kenny, G., Henrichs, I., & Mulligan, D. (2020). The trace element composition of apatite and its application to detrital provenance studies. *Earth-Science Reviews*, *201*, 103044. https://doi.org/10.1016/j.earscirev.2019.103044

O'Sullivan, G. J., Chew, D. M., Morton, A. C., Mark, C., & Henrichs, I. A. (2018). An integrated apatite geochronology and geochemistry tool for sedimentary provenance analysis. *Geochemistry, Geophysics, Geosystems*, *19*(4), 1309–1326. https://doi.org/10.1002/2017GC007343

Paton, C., Hellstrom, J., Paul, B., Woodhead, J., & Hergt, J. (2011). Iolite: Freeware for the visualization and processing of mass spectrometric data. *Journal of Analytical Atomic Spectrometry*, *26*(12), 2508–2518. https://doi.org/10.1039/C1JA10172B

Pullen, A., Banaszynski, M., Kapp, P., Thomson, S. N., & Cai, F. (2020). A mid-cretaceous change from fast to slow exhumation of the western Chinese Altai Mountains: A climate driven exhumation signal? *Journal of Asian Earth Sciences*, *197*, 104387. https://doi.org/10.1016/j.jseaes.2020.104387

Schoene, B., & Bowring, S. A. (2006). U-Pb systematics of the McClure mountain syenite: Thermochronological constraints on the age of the ^{40}Ar/^{39}Ar standard MMhb. *Contributions to Mineralogy and Petrology*, *151*(5), 615–630. https://doi.org/10.1007/s00410-006-0077-4

Sláma, J., Košler, J., Condon, D. J., Crowley, J. L., Gerdes, A., Hanchar, J. M., et al. (2008). Plešovice zircon—A new natural reference material for U–Pb and Hf isotopic microanalysis. *Chemical Geology*, *249*(1), 1–35. https://doi.org/10.1016/j.chemgeo.2007.11.005

Sobel, E. R., Chen, J., & Heermance, R. V. (2006). Late Oligocene–early Miocene initiation of shortening in the southwestern Chinese Tian Shan: Implications for Neogene shortening rate variations. *Earth and Planetary Science Letters*, *247*(1), 70–81. https://doi.org/10.1016/j.epsl.2006.03.048

Sun, M., Yuan, C., Xiao, W., Long, X., Xia, X., Zhao, G., et al. (2008). Zircon U–Pb and Hf isotopic study of gneissic rocks from the Chinese Altai: Progressive accretionary history in the early to middle Palaeozoic. *Chemical Geology*, *247*(3), 352–383. https://doi.org/10.1016/j.chemgeo.2007.10.026

Thomas, J. C., Lanza, R., Kazansky, A., Zykin, V., Semakov, N., Mitrokhin, D., & Delvaux, D. (2002). Paleomagnetic study of Cenozoic sediments from the Zaisan Basin (SE Kazakhstan) and the Chuya depression (Siberian Altai): Tectonic implications for central Asia. *Tectonophysics*, *351*(1–2), 119–137. https://doi.org/10.1016/S0040-1951(02)00128-2

Thomson, S. N., Gehrels, G. E., Ruiz, J., & Buchwaldt, R. (2012). Routine low-damage apatite U-Pb dating using laser ablation-multicollector-ICPMS. *Geochemistry Geophyeophysics Geosystems*, *13*(2), Q0AA21. https://doi.org/10.1029/2011GC003928

Tong, Y., Wang, T., Jahn, B.-m., Sun, M., Hong, D.-W., & Gao, J.-F. (2014). Post-accretionary Permian granitoids in the Chinese Altai orogen: Geochronology, petrogenesis and tectonic implications. *American Journal of Science*, *314*(1), 80–109. https://doi.org/10.2475/01.2014.03

van der Beek, P. A., Delvaux, D., Andriessen, P. A. M., & Levi, K. G. (1996). Early Cretaceous denudation related to convergent tectonics in the Baikal region, SE Siberia. *Journal of the Geological Society*, *153*(4), 515–523. https://doi.org/10.1144/gsjgs.153.4.0515

Vassallo, R., Jolivet, M., Ritz, J. F., Braucher, R., Larroque, C., Sue, C., et al. (2007). Uplift age and rates of the Gurvan Bogd system (Gobi-Altay) by apatite fission track analysis. *Earth and Planetary Science Letters*, *259*(3–4), 333–346. https://doi.org/10.1016/j.epsl.2007.04.047

Vermeesch, P. (2017). Statistics for LA-ICP-MS based fission track dating. *Chemical Geology*, *456*, 19–27. https://doi.org/10.1016/j.chemgeo.2017.03.002

Vermeesch, P. (2018). IsoplotR: A free and open toolbox for geochronology. *Geoscience Frontiers*, *9*(5), 1479–1493. https://doi.org/10.1016/j.gsf.2018.04.001

Vincent, S. J., & Allen, M. B. (2001). *Sedimentary record of Mesozoic intracontinental deformation in the eastern Junggar Basin, northwest China: Response to orogeny at the Asian margin* (pp. 341–360). Geological Society of America.

Wagner, G. A., Gleadow, A. J. W., & Fitzgerald, P. G. (1989). The significance of the partial annealing zone in apatite fission-track analysis: Projected track length measurements and uplift chronology of the Transantarctic Mountains. *Chemical Geoscience*, *79*(4), 295–305. https://doi.org/10.1016/0168-9622(89)90035-3

Wagner, G. A., & Reimer, G. M. (1972). Fission track tectonics: The tectonic interpretation of fission track apatite ages. *Earth and Planetary Science Letters*, *14*(2), 263–268. https://doi.org/10.1016/0012-821X(72)90018-0

Wang, Q., Li, S., & Du, Z. (2009). Differential uplift of the Chinese Tianshan since the cretaceous: Constraints from sedimentary petrography and apatite fission-track dating. *International Journal of Earth Sciences*, *98*(6), 1341–1363. https://doi.org/10.1007/s00531-009-0436-2

Wang, T., Jahn, B. M., Kovach, V. P., Tong, Y., Wilde, S. A., Hong, D. W., et al. (2014). Mesozoic intraplate granitic magmatism in the Altai accretionary orogen, NW China: Implications for the orogenic architecture and crustal growth. *American Journal of Science*, *314*(1), 1–42. https://doi.org/10.2475/01.2014.01

Wang, W., & Chen, Y. (2004). Tectonic evolution and petroleum systems in the Junggar Basin. *Acta Geologica Sinica-English Edition*, *78*(3), 667–675. https://doi.org/10.1111/j.1755-6724.2004.tb00181.x

Wang, Y. N., Cai, K. D., Sun, M., Xiao, W. J., De Grave, J., Wan, B., & Bao, Z. H. (2018). Tracking the multi-stage exhumation history of the western Chinese Tianshan by apatite fission track (AFT) dating: Implication for the preservation of epithermal deposits in the ancient orogenic belt. *Ore Geology Reviews*, *100*, 111–132. https://doi.org/10.1016/j.oregeorev.2017.04.011

Windley, B. F., Alexeiev, D., Xiao, W., Kroener, A., & Badarach, G. (2007). Tectonic models for accretion of the central Asian orogenic belt. *Journal of the Geological Society*, *164*(1), 31–47. https://doi.org/10.1144/0016-76492006-022

Windley, B. F., Kröner, A., Guo, J., Qu, G., Li, Y., & Zhang, C. (2002). Neoproterozoic to Paleozoic geology of the Altai Orogen, NW China: New zircon age data and tectonic evolution. *The Journal of Geology*, *110*(6), 719–737. https://doi.org/10.1086/342866

Xiao, W., Windley, B. F., Sun, S., Li, J., Huang, B., Han, C., et al. (2015). A tale of amalgamation of three Permo-Triassic collage systems in Central Asia: Oroclines, sutures, and terminal accretion. *Annual Review of Earth and Planetary Sciences*, *43*(1), 477–507. https://doi.org/10.1146/annurev-earth-060614-105254

Xiao, W. J., Windley, B. F., Yuan, C., Sun, M., Han, C. M., Lin, S. F., et al. (2009). Paleozoic multiple subduction-accretion processes of the southern Altaids. *American Journal of Science*, *309*(3), 221–270. https://doi.org/10.2475/03.2009.02

Xue, C. J., Chi, G. X., Zhao, X. B., Wu, G. G., Zhao, Z. F., & Dong, L. H. (2016). Multiple and prolonged porphyry Cu-Au mineralization and alteration events in the Halasu deposit, Chinese Altai, Xinjiang, northwestern China. *Geoscience Frontiers*, *7*(5), 799–809. https://doi.org/10.1016/j.gsf.2015.10.008

Yin, C., Ou, J., Long, X., Huang, F., Zhang, J., Li, S., et al. (2019). Late Cretaceous Neo-Tethyan slab roll-back: Evidence from zircon U-Pb-O and whole-rock geochemical and Sr-Nd-Fe isotopic data of adakitic plutons in the Himalaya-Tibetan Plateau. *GSA Bulletin*, *132*(1–2), 409–426. https://doi.org/10.1130/b35242.1

Yuan, W. M., Carter, A., Dong, J. Q., Bao, Z. K., An, Y. C., & Guo, Z. J. (2006). Mesozoic-tertiary exhumation history of the Altai Mountains, northern Xinjiang, China: New constraints from apatite fission track data. *Tectonophysics*, *412*(3–4), 183–193. https://doi.org/10.1016/j.tecto.2005.09.007

Zhang, C.-L., Santosh, M., Zou, H.-B., Xu, Y.-G., Zhou, G., Dong, Y.-G., et al. (2012). Revisiting the "Irtish tectonic belt": Implications for the Paleozoic tectonic evolution of the Altai orogen. *Journal of Asian Earth Sciences*, *52*, 117–133. https://doi.org/10.1016/j.jseaes.2012.02.016

Zhang, Z., Zhu, W., Zheng, D., Zheng, B., & Yang, W. (2016). Apatite fission track thermochronology in the Kuluketage and Aksu areas, NW China: Implication for tectonic evolution of the northern Tarim. *Geoscience Frontiers*, *7*(2), 171–180. https://doi.org/10.1016/j.gsf.2015.08.007

Zhang, Z. Y., Zhu, W. B., Shu, L. S., Wan, J. L., Yang, W., Su, J. B., & Zheng, B. H. (2009). Apatite fission track thermochronology of the Precambrian Aksu blueschist, NW China: Implications for thermo-tectonic evolution of the north Tarim basement. *Gondwana Research*, *16*(2), 182–188. https://doi.org/10.1016/j.gr.2009.04.006

Zheng, Y., Chen, Y. J., Cawood, P., Wang, Y. J., Chen, H. Y., Zhang, L., & Li, D. F. (2017). Late Permian-Triassic metallogeny in the Chinese Altay Orogen: Constraints from mica $^{40}Ar/^{39}Ar$ dating on ore deposits. *Gondwana Research*, *43*, 4–16. https://doi.org/10.1016/j.gr.2015.08.018

Zhou, Q., Qin, K., Tang, D., Tian, Y., Cao, M., & Wang, C. (2015). Formation Age and evolution Time span of the Koktokay No. 3 pegmatite, Altai, NW China: Evidence from U–Pb zircon and ^{40}Ar–^{39}Ar Muscovite ages. *Resource Geology*, *65*(3), 210–231. https://doi.org/10.1111/rge.12067

References From the Supporting Information

Ketcham, R. A., Carter, A., Donelick, R. A., Barbarand, J., & Hurford, A. J. (2007). Improved modeling of fission-track annealing in apatite. *American Mineralogist*, *92*(5–6), 799–810. https://doi.org/10.2138/am.2007.2281